ACS OMEGA

http://pubs.acs.org/journal/acsodf

Article

Biodiesel Production from Transesterification with Lipase from Pseudomonas cepacia Immobilized on Modified Structured Metal Organic Materials

José Manuel Martínez Gil, Ricardo Vivas Reyes, Marlon Bastidas-Barranco, Liliana Giraldo, and Juan Carlos Moreno-Piraján*

Cite This: *ACS Omega* 2022, 7, 41882−41904

Read Online

ACCESS | Metrics & More | Article Recommendations

ABSTRACT: This research presents the modification of MOF-199 and ZIF-8 using furfuryl alcohol (FA) as a carbon source to subsequently fix lipase from *Pseudomonas cepacia* and use these biocatalysts in the transesterification of African palm oil (APO). The need to overcome the disadvantages of free lipases in the biodiesel production process led to the use of metal organic framework (MOF)-type supports because they provide greater thermal stability and separation of the catalytic phase, thus improving the activity and efficiency in relation to the use of free lipase, disadvantages that could not be overcome with the use of other types of catalysts used in transesterification/esterification reactions for the production of biodiesel. The modification of MOFs ZIF-8 and MOF-199 with FA increases the pore volume which allows better immobilization of *Pseudomonas cepacia* lipase (PCL). The results show that these biocatalysts undergo transesterification with biodiesel yields above 90%. Additionally, studies were carried out on the effect of (1) enzyme loading, 2) enzyme immobilization time, (3) enzyme immobilization temperature, and (4) pH on the % immobilization of the enzyme and the specific activity. The results show that the highest immobilization efficiency for the FA@ZIF-8 support has a value of 91.2% when the load of this support was 3.5 mg/mg and has a specific activity of 142.5 U/g protein. The FA@MOF-199 support presented 80.3% enzyme immobilization and 125% U/g specific activity protein. We established that the specific activity increases in the period from 0.5 to 5.0 h for the systems under investigation. After this time, both the specific activity and the % efficiency of enzyme immobilization decrease. Therefore, 5.0 h (immobilization efficiency of 95 and 85% for FA@MOF-199, respectively) was chosen as the most appropriate time for PCL immobilization. Methods of adding methanol, with three and four steps, were tested, where biodiesel yields greater than 90% were obtained for the biocatalysts synthesized in this work (FA@ZIF-8-PCL and FA@MOF-199-PCL) and above 70% for free PCL, and the maximum yield was reached at a molar ratio between methanol and APO of 4:1 when using the one-step method under the same reaction conditions (as mentioned above). Only the results of FA@ZIF-8-PCL are presented here; however, it should be noted that the results for biocatalyst FA@MOF-199-PCL and lipase-free PCL presented the same behavior. The order of biocatalyst performance was FA@ZIF-8-PCL > FA@MOF-199-PCL > PCL-Free, which demonstrates that the use of FA as a modifier is a novel aspect in the conversion of palm oil into biodiesel components.

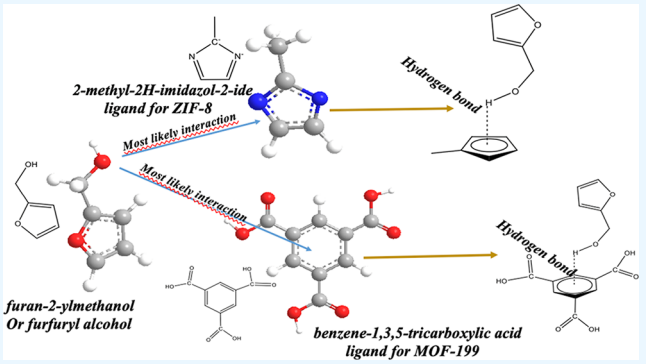

1. INTRODUCTION

Industrial development has been based on the very high consumption of fuels, which are used in a vast majority of chemical process activities. This has generated great concern about environmental safety not only due to the high consumption but also due to the activities generated due to this consumption, such as transport of large quantities which can generate environmental danger in case of spills, in addition to the multiple industrial applications which have resulted in the depletion of fossil fuel reserves. This has posed a great challenge to the scientific community which has focused its research in this area in order to find alternative energy sources to synthesize liquid fuels that are renewable and, most importantly, nontoxic and environmentally friendly.[1−3]

Numerous investigations have found the so-called agrodiesel, green biodiesel, or simply biodiesel to be an excellent substitute

Received: May 9, 2022
Accepted: September 28, 2022
Published: November 8, 2022

for conventional fuels, and it has additionally shown to be very promising, particularly when compared to conventional diesel derived from petroleum due to its renewable nature, low exhaust gas emission, high ignition, nontoxicity, biodegradability, and use in recycling carbon dioxide (CO_2) in short periods.[2−5] Producing biodiesel additionally has an additional plus and is that it is very friendly to the environment because it is possible to use residues of vegetable oils and fats during its synthesis process, reducing pollution due to the poor handling of residues such as frying oils, fats that are discarded, and so forth.[3−5] When an adequate synthesis is carried out to obtain a good-quality biodiesel, its use varies, and it can be used directly in the currently existing compression ignition engines (diesel) and in refueling technology without the need to previously modify the injection system or the engine or the fuel lines due to its physically adjustable ability and chemical properties.[2−7]

Monoalkyl esters of long-chain fatty acids are the main components of green biodiesel, which highlights that it is a green fuel not derived from petroleum but produced from the oil of plants, vegetables, waste, microorganisms, and animal fats through a transesterification reaction.[2,8,9] When combined, 1 mol triglyceride reacts with 3 mol short-chain alcohol (ethanol or methanol) in the presence of a suitable catalyst to produce biodiesel,[2,3,10,11] and thus, transesterification is accelerated.

To carry out transesterification, researchers use both homogeneous catalysts and heterogeneous catalysts for the production of biodiesel. Due to the faster reaction rate, acidic and/or basic homogeneous solid catalysts are commonly used in the industrial production of biodiesel under mild reaction conditions.[2,3,12] The corrosive nature, the increase in pH of the final product, the generation of emulsion, the reuse or regeneration of the catalysts, and the involvement of a large amount of wastewater processing are the main problems with the use of a homogeneous catalyst for biodiesel production.[2,3,13] This coupled with the difficulty of separating the catalysts from the methyl ester phase and requirement for faster equipment and skilled labor results in higher production costs. To overcome these drawbacks, it has been reported that a heterogeneous base−acid catalyst such as KOH/Al_2O_3 and alumina/silica for the transesterification reaction is an alternative solution to the conventional homogeneous catalysts.[2,3,14] The type of catalysts designed in this way follows (during the separation process) an easier step, provides a product free of catalyst impurities, and follows steps of neutralization and purification of the product, therefore improving the purity of the reaction products.[2,3,15] However, chemical process materials dissolved in methanol are relatively difficult to synthesize and even hinder the recovery of glycerol from biodiesel.[2,3,16] Acid catalysts use a higher methanol/oil molar ratio and require a longer reaction time. Several alternatives have been proposed with the aim of overcoming the aforementioned drawbacks during transesterification, and one of the alternative techniques is based on enzymatic processes for the production of biodiesel, taking into account that it is a very promising and additionally ecological technique.[2,17]

It is worth noting that the synthesis of biodiesel by enzymatic biocatalysis has an added value such as the reduction of waste generation and CO_2 emission compared to those from fossil fuels due to its substrate specificity. Lipases (triacylglycerol ester hydrolase, EC 3.1.1.3) are considered as a type of green catalyst that is produced by plants, animals, and microorganisms and have wide applications depending on the type or class to which they belong, having a broad spectrum of applications both at commercial and industrial levels, logically including the transesterification process.[2,3,18−21] Thus, lipases from different sources are the most common enzymes for transesterification and biodiesel production from lipids.[2,3,22,23]

Although the use of lipases is promising, their application in the free form in the production of biodiesel is limited due to several factors such as inactivation of enzymatic activity, regular stability, % recycling, and reuse. Enzyme immobilization techniques have been studied, a procedure that is very important when evaluating the reaction products that are catalyzed by the respective enzyme, and these techniques play a critical and beneficial role in the formation of products and usually overcome the aforementioned weak points effectively.[2,3,24,25]

Is it possible to increase certain properties of enzymes such as activity, thermal stability, and subsequent reuse using the correct immobilization technique? However, this is possible if the enzymes are supported on a suitable porous solid that allows their properties to be maintained and/or increased during the particular transesterification process.[2,3,26] In the scientific literature, several authors have reported a wide variety of porous materials to support lipases, such as calcite,[27] activated carbon,[17] chitosan,[28] graphene oxide (GO),[29] magnetite nanoparticles,[30] silica gel,[31] resins,[2,3,32] polyurethane,[3,33] and zeolite.[2,3,34] On the other hand, metal−organic frameworks (MOFs) are a class of novel porous materials which are formed by organic ligands and inorganic metal nodes assembled by coordination bonds.[35,36] Their design is varied due to the great diversity of organic ligands and metal ions, as well as the way of combining and generating diverse structures; MOF materials have a great variety of types. Due to their textural properties, diverse crystal structures, controllable pore size, high porosity, and specific surface area,[37] MOFs are nowadays widely investigated structures. MOFs are materials that, according to the synthesis routes, can be applied in various areas such as adsorption separation,[38] photoelectric induction,[35,39] biotechnology,[40] and so forth. Carrying out the immobilization of enzymes on porous solid supports of different characteristics usually generates low protein loading efficiency,[41] low stability at high temperatures, and enzymatic leaching.

Therefore, zeolitic imidazolate frameworks (ZIFs) are a class of supports worth investigating as possible supports for enzyme immobilization on various MOFs.[42−44] The scope of this research is to explore the scope of the use of MOF-199 and ZIF-8 as lipase supports from *Pseudomonas cepacia* in the transesterification reaction for the synthesis of green biodiesel from African palm oil (APO). Additionally, the modification of the two MOFs by means of furfuryl alcohol (FA) is studied, and they are supported on these *Pseudomonas cepacia* lipase (PCL) materials, and the biodiesel production capacity is evaluated. In this work, the effect of temperature, pH, lipase dosage, and time is investigated. To make comparisons, this study is based on published research on the same subject.[45]

The biocatalysts are characterized by N_2 isotherms at 77 K, X-ray diffraction (XRD), Fourier transform infrared (FTIR) spectroscopy, and scanning electron microscopy (SEM)-energy-dispersive X-ray spectroscopy (EDS).

2. EXPERIMENTAL METHODOLOGY

2.1. Characterization of the Starting Adsorbents.

2.1.1. Reagents Used. MOF-199 and ZIF-8 (Sigma-Aldrich), *Pseudomonas cepacia* from lipase (Sigma-Aldrich (62309)), methanol (Merck), FA (Sigma-Aldrich, 185930), and APO (certified by the National Federation of Oil Growers, FedePalma) were used.

https://doi.org/10.1021/acsomega.2c02873
ACS Omega 2022, 7, 41882−41904

2.1.2. Modification of MOFs with FA. FA, MOF-199, and ZIF-8 were introduced as additional carbon sources by the impregnation method. The procedure reported in the literature[45] was closely followed with some small changes according to previous experiments carried out in our laboratory with the aim of optimizing the modification of the MOFs. In summary, initially, 4.5 g of both MOFs (MOF-199 and ZIF-8) was dissolved in 40 mL of FA solution and stirred for 20 min. Each mixture was then kept at room temperature without stirring overnight, and finally, each product was separated by filtration and labeled FA@MOF-199 and FA@ZIF-8, respectively.

2.1.3. TGA of MOFs. Differential thermal analysis (DTA) and thermogravimetric analysis (TGA) were performed on a Hitachi STA7000 series simultaneous thermal analysis instrument. Approximately 10−20 mg of each of the MOF samples was placed in a platinum crucible on the plate of a microbalance and then heated from room temperature to 800 °C at a heating rate of 2 °C/min while purging with argon at a flow of 100 mL min^{-1} and constantly weighed.

2.1.4. FTIR Spectrophotometry. The FTIR absorbance spectra of the MOFs were recorded using the KBr technique, with analysis performed on a Nicolet iS 50 FTIR spectrometer in the wavenumber range of 4000−400 cm^{-1}. The solid samples were mixed with KBr in a ratio of approximately 1:300, and then, the mixture was ground in an agate mortar to a very fine powder. After drying at 100 °C for 12 h in a vacuum oven, about 300 mg of the fine powder was used to make a pellet. After preparation, the pellet was immediately analyzed, and the spectra were recorded by a series of scans with a resolution of 4 cm^{-1}. A pellet prepared with an equivalent amount of pure KBr powder was used as the background.

2.1.5. SEM-EDS of the MOFs. Analyses of the morphology, chemical composition, and elemental maps of the samples were performed using a JEOL JSM-7100FA field-emission scanning electron microscope equipped with an energy-dispersive X-ray system.

2.1.6. X-ray Diffraction. Powder XRD patterns were recorded on an X-ray diffractometer (MiniFlex II, Rigaku, Japan) at 30 kV and 15 mA using Cu Ka radiation (λ = 1,5418 Å), with a scan rate of 4° min^{-1}, a step size of 0.01° in 2 h, and a sweep range of 3−40°.

2.1.7. Isotherms of N_2 at 77 K. The textural characterization of the starting materials and those modified with furfuric acid was carried out. The preliminary texture of the materials was determined by physical adsorption on N_2 at 77 K using a Quantachrome IQ2 sorptometer. The results of the gas−solid isotherms were analyzed in different pressure ranges using the Brunauer−Emmett−Teller (BET) method in which the calculation of the specific surface area (P/P^o range) was determined using the method proposed by Rouquerol et al.[46,47] Dubinin−Astakhov (DA) for micropore analysis (P/P^o range< 0.1) and narrow micropore volume, pores <0.7 nm, was calculated by applying the DA equation to CO_2 adsorption data at 0 °C and density functional theory (DFT; range P/P^o 10^{-7}−1) considering different pore models and the effects of surface roughness and heterogeneity nonlocal DFT (NLDFT) and quenched solid (QSDFT) using the ASQiWin software.[46]

2.2. Lipase Preparation from PCL Tuned. 100 mg of *PCL* was weighed and dissolved in 0.5 mL of 20 mM sodium phosphate buffer, pH 8.00. This solution thus corresponds to what we will call tuned lipase here.

2.3. Transesterification Reaction from Supported *PCL* + Methanol. We carried out the respective transesterification reactions using the free-lipase enzyme from PCL and with the enzyme supported on the FA-modified MOFs, which are labeled in this study as FA@MOF-199-PCL and FA@ZIF-8-PCL. The samples were stored in a humidity-free environment until use. Methanol was used as a solvent for the process and APO as raw materials.

2.4. Procedure for Performing the Lipase Immobilization Optimization Study (PCL) on MOFs by the Simple Physical Adsorption Method as a Function of pH, Temperature, Time, and Amount of Lipase from *PCL*. Initially, in order to study the optimal conditions for the immobilization of *PCL*on the different supports in an adequate manner, previous tests were carried out in order to establish these conditions based on the (1) pH, (2) temperature, (3) time, and (4) amount of lipase for its immobilization. To determine the effect of pH on the immobilization of lipase from *PCL*, 20 mM sodium phosphate buffer was used at pH 5.0 6.0; 7.0, 8.0, 9.0, and 10.0. To study the effect of temperature, 125 mg of the respective supports (MOF-199 and ZIF-8) was suspended in the solution of lipase from *PCL*(100 mg of *PCL*, dissolved in 0.5 mL of 20 mM sodium phosphate buffer pH 7.0) at different temperatures (4, 25, 37, 60, and 70 °C) for 6 h; then, it was centrifuged at 5000 rpm, establishing that the volume of the supernatant was 95% with respect to the original solution of *PCL*. Finally, the effect of incubation time on the immobilization of the lipase from *Pseudomonas cepacia* was also studied, for which small aliquots were withdrawn for a period of time, and the solutions were centrifuged, and the supernatant (lipase from *Pseudomonas cepacia*) was stored at 5 °C. Catalysts with supported lipases were labeled: FA@MOF-199-PCL and FA@ZIF-8-PCL.

2.5. Preparation of the Immobilized Enzyme. The tuned PCL prepared in Section 2.2. was mixed with 125 mg of each support (FA@MOF-199 and FA-ZIF-8) and subsequently brought to −20 °C and lyophilized for 48 h. After 24 h and performing constant agitation at 250 rpm, the respective support was removed; the residual liquid was stored to evaluate the amount of protein. Sodium phosphate (pH 7) washes were performed, with 2 to 5 min for each wash session. Then, the two biocatalysts (FA@MOF-199 and FA-ZIF-8) were stored in a freezer at 5 °C. Wash solutions were stored to determine their protein content.

The amount of enzyme immobilized on the supports was evaluated by measuring the concentrations of the initial enzyme solution (milligram of initial protein) and the concentration of the supernatant and washing solutions (milligram of final protein) using the Bradford method.

2.6. Enzymatic Activity of *PCL*. The activity of the lipase from free and immobilized *Pseudomonas cepacia* was determined using palmitic fatty acid (PFA) as a substrate (one of the fatty acids that has the greatest quantity in APO), and a reaction mixture was prepared, which contained 75 μL of FA (20 mM) and 5 μL of *PCL,* and 20 mM sodium phosphate buffer pH 8.00 was made up to a volume of 3 mL, and this was done for both the biocatalysts (FA@MOF-199-PCL and FA@ZIF-PCL) and the free enzyme (PCL). Subsequently, they were incubated at 37 °C for 15 min, and the reaction was terminated by adding 1 mL of 0.2 M sodium carbonate. The synthesized biodiesel was subsequently quantified.

https://doi.org/10.1021/acsomega.2c02873
ACS Omega 2022, 7, 41882−41904

One unit (U) of enzyme activity was defined as the amount of enzyme that produced 1 μmol FAME in 1 min under the assay conditions.

2.7. Optimization of the Parameters for the Fixation of the Lipase from Free *Pseudomonas cepacia* and the MOFs for Its Subsequent Use in the Transesterification of Palm Oil. To carry out this procedure, APO (0.5 g) and methanol were taken in a ratio of 1:4 (mol^{-1}) in a glass vial with a screw cap. To this mixture, 50 mg of the prepared enzyme (refined or immobilized) was added and then incubated at 40 °C with constant agitation at 200 rpm. The progress of the reaction was monitored by withdrawing aliquots (20 μL) at various time intervals. Aliquots were diluted appropriately (with hexane), and lauric acid was added to the diluted aliquots as an internal standard prior to gas chromatography (GC) analysis.

2.8. Biodiesel Quantification. Fuel characteristics were verified by European (EN) and American Society for Testing and Materials (ASTM) standards. Based on these, the following properties were determined: acidity, pH, density, calorific value, humidity, and percentage of esters.

2.8.1. Characterization of Biodiesel. 2.8.1.1. Density. It was determined using a pycnometer at 20 °C, and then according to the provisions of the EN 14214 standard, we have

$$\rho_{15\,^\circ C} = \rho_T + 0{,}723 \times (T - 15)$$

where$\rho_{15°C}$ = density at 15 °C in $Kgm^{-3}\rho_T$ = density in °C y Kgm^{-3} of certain temperature.

2.8.1.2. Humidity. It was determined by performing TGA using the STA 7200 Hitachi High Tech equipment and TAT 7200 Standard Analysis software using 10.0 mg of the sample and a temperature ramp of 10 °C.min^{-1}, starting at 30 °C and ending at 500 °C, in a nitrogen atmosphere with a flow of 100 mL min^{-1}.

2.8.1.3. Determination of the Acid Value. It is defined as the amount (in milligrams) of potassium hydroxide required to neutralize the free fatty acids contained in 1.0 g of the sample. The method was based on the EN 14104 and ASTM D774 standards: the samples were dissolved in hot, neutralized alcohol, and the free fatty acids that were solubilized in hot, neutralized alcohol were determined by means of titration with potassium hydroxide.

The method was as follows:

a 1.0 mL of 96% ethanol was taken; two drops of phenolphthalein were added; and the solution was heated and neutralized with 0.1 N potassium hydroxide.

b 0.5 g of the sample was added, mixed, and titrated with 0.1 N KOH. This was performed in triplicate; the percentage of acidity is given by the average according to

$$\text{Acidity Index} = \frac{V_{KOH} \times N_{KOH} \times M_{KOH}}{m}$$

whereV_{KOH} = volume in milliliter of KOH spent in the titration.N_{KOH} = KOH normality.M_{KOH} = molecular weight of KOH in g $mol.^{-1}m$ = weighted amount of the sample.

2.8.1.4. Saponification Value. According to the ASTM 1962−95 standard, it is expressed as the weight in milligram of KOH necessary to saponify 1.0 g of the sample.

The method is as follows:

a 1 g of the sample was weighed.

b 15 mL of 0.5 KOH was added.

c heated for 1 h under reflux.

d Once this time had elapsed, two drops of phenolphthalein were added, and the solution was titrated with 0.5 M HCI.

e The same process was repeated with a blank sample

$$\text{Saponification index} = \frac{M_{KOH} \times M_{HCl} \times (V_b - V_m)}{m_b}$$

whereM_{KOH} = molecular weight of KOH in g $mol.^{-1}M_{HCl}$ = concentration of the HCI solution.V_h = volume in milliliter of HCI spent in the titration of the blank.V_m = volume in milliliter of HCI spent in the titration of the sample.m_b = weighted amount of the sample.

2.8.1.5. Viscosity. The determination of the viscosity was carried out at 40 °C according to the ASTM D445 standard using an Ostwald viscometer.

$$\mu = K \times t$$

whereμ = kinematic viscosity in cSt.K= viscometer constant.t = time it takes for the liquid to fall.

2.8.1.6. Cetane Index. A FOSS brand near-IR (NIR) spectrophotometry equipment was used. Measurements were performed at room temperature, initially using air as a blank.

2.8.1.7. Calorific Power. The calorific value was measured using a 1341 Parr oxygen bomb calorimeter, with Parr 45c10 nickel-chromium wise, and excess oxygen in combustion at a rate of 25 Atm. For the calculation, the heat of combustion of the wire was considered to be 2.3 cal/cm, and a specific heat of the pump equivalent to 2430 cal. $°C^{-1}$ according to the pump's user manual. For its calibration, a 1.0 g benzoic acid pellet for calorimetric combs (CAS reg N. 65-85-0) was used, which must present a temperature increase of 3 °C.

Determination of Characteristics According to European Standard EN 1421: Biodiesel needs to have specifications that list the properties and guarantee the quality of the product. In addition, biodiesel must meet the requirements for mineral automotive fuels, which are set out in the European standard EN-590. In this research, in parallel, the parameters recommended by the European standard to ensure the quality of the synthesized biodiesel were determined. This standard is EN-14214 (2003), which brings together and specifies all the test methods to be followed for methyl esters of the corresponding fatty acids that are currently marketed and used for automotive engines in concentrations up to 100%. The parameters density, moisture, acid value, viscosity, cetane number, calorific value, and flash point were determined according to EN ISO 3675, EN ISO 12185, EN ISO 12937, EN 14104, EN ISO 3104, EN ISO 5165, and EN ISO CD 3679e, respectively.

2.8.1.8. Gas Chromatography. Methyl esters (from biodiesel FAMEs) were analyzed by means of GC coupled to a mass spectrometer (Shimadzu series QP2010S) with a medium−high polarity type column (DB-225 MS, Agilent, serial N US5268413H) with dimensions 20 m × 0.1 mm × 0.1 μm. The conditions set for the analysis were as follows: mass injector temperature = 220 °C, using helium as the carrier gas with a flow rate of 1.0 mL/min, sample injection = 1.0 μL, automatic sample chromatographic series (AOC) injection = 20 s (split mode, using a 30:1 ratio). The temperature program followed in the oven was follows: initial temperature 60.0 °C for 1 min, then heating at 10 °C/min up to 195 °C, after reaching this temperature, heating from 3.0 °C min^{-1} up to 205 °C, and finally 8.0 °C min^{-1} until 220 °C; this temperature was maintained for 30 min before ending the analysis.

https://doi.org/10.1021/acsomega.2c02873
ACS Omega 2022, 7, 41882−41904

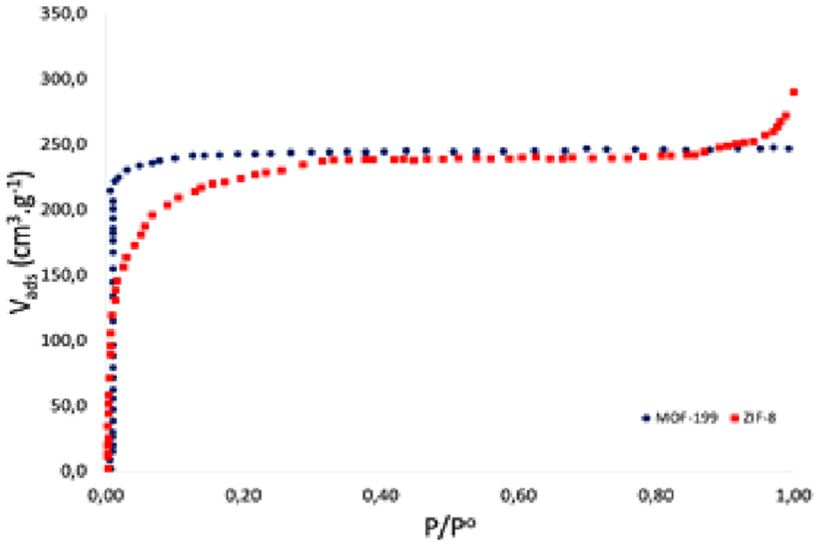

Figure 1. N_2 adsorption−desorption isotherms MOF-199 (blue circles) and ZIF-8 (red circle).

Table 1. DA and DFT Parameters Obtained from the Adsorption−Desorption Isotherm of N_2 at 77.4 K

		DA ($P/P°$< 0.1)			DFT ($P/P°$ 10^{-7}−1)		
samples	S_{BET} [m^2 g^{-1}]*	V_{mic} [cm^3 g^{-1}]	E_o [Kj mol^{-1}]	n	pore radius [Å]	V_P [cm^3 g^{-1}]	half pore width [Å]
MOF-199	1750	0.66	8.47	3.4	7.0	0.69	3.52
ZIF-8	1733	0.88	4.47	3.4	8.6	0.65	4.63

Quantification was performed by area optimization and using internal standards. Methyl-heptadecanoate (Sigma-Aldrich, reference 51633-1G) was used as an internal standard; a calibration curve was plotted from 10 to 500 ppm, and with it, the different biodiesel samples were quantified. For the identification of methyl esters, two mixtures of FAMEs, Supelco (GLC 30 and GLC90), from C8:0 to C21:0 were used.

2.8.2. Transesterification. 2.8.2.1. Lipase-Catalyzed Transesterification from Pseudomonas cepacia. Studies were carried out with the three systems: free PCL and the synthesized biocatalysts (FA@MOF-199-PCL and FA@ZIF-8-PCL). APO (0.5 g) and methanol were taken in a ratio of 1:4 (mol^{-1}) in a screw cap vial. 50 mg of each biocatalyst synthesized in this work was added to this mixture: FA@MOF-199-PCL, FA@ZIF-8-PCL, and free PCL; then, they were incubated at 40 °C with constant agitation at 200 rpm. The progress of the reaction was monitored by withdrawing aliquots (10 μL) at various time intervals. Aliquots were diluted appropriately (with hexane), and lauric acid was added as an internal standard to the diluted aliquots before analysis by GC.

2.8.2.2. Effect of the Amount of Each Biocatalyst, FA@MOF-199-PCL and FA@ZIF-8-PCL, in the Transesterification Reaction in the Presence of Methanol. APO (0.5 g) and 2.0 mL of methanol were taken and placed in a screw cap vial. Varying amounts of each biocatalyst, FA@MOF-199 and FA@ZIF-8, were added to this mixture separately, namely, 10, 50, 75, and 100 mg. The reaction mixture was incubated at 40 °C with constant stirring at 270 rpm for 8 h. Aliquots were diluted appropriately (with hexane), and the corresponding internal standards were added to the diluted aliquots prior to analysis by GC.

Each of the above reactions was performed in duplicate, and the yields between duplicate experiments were found to be within 3%.

3. RESULTS

3.1. Results of the Unmodified Supports: Textural Analysis of the Starting MOF-199 and ZIF-8. The morphological properties of MOF-199 and ZIF-8 were determined by nitrogen adsorption analysis at 77.0 K. The results show that the commercial starting MOFs present type I isotherms, according to recent IUPAC recommendations, which are shown in Figure 1. A detailed analysis of these adsorption−desorption isotherms of these starting MOFs shows a microporous network for ZIF-8 (pore size <2 nm). If the area of study of the isotherm at low pressure is extended for this ZIF-8, it is observed that it has a slight change in the trend of the isotherm corresponding to type VI behavior. This phenomenon has already been analyzed in the scientific literature, which, according to the researchers, is explained by a possible structural flexibility that is induced by the gas on the ZIF-8 structure, while some authors argue that this behavior is due to the very weak interaction between the adsorbate and adsorbent. The literature has also reported this interesting phenomenon.[48−50] The microporous volume is 0.88 cm^3 g^{-1} as calculated by applying the DA method. The synthesized sample is a microporous material with a BET specific surface of 1750 m^2 g^{-1} (relative pressure calculated from 0.009 to 0.02).

The textural properties for the two starting materials are summarized in Table 1.

The evaluation of the parameters reveals that the two materials used in the subsequent synthesis of the biocatalysts have high BET specific surface areas,[51−54] which are slightly higher than those reported in the technical data sheet of the manufacturer.

This is probably due to the fact that they were previously subjected to a study of the effect of drying on their BET area, and thus, an adequate temperature and the level of vacuum were selected for desorption (so that the structure would not be

https://doi.org/10.1021/acsomega.2c02873
ACS Omega 2022, 7, 41882−41904

affected). In this investigation, detailed studies were carried out on the other textural parameters. It was found that for MOF-199, the micropore volume is 0.66, and for ZIF-8, it is 0.88 $cm^3\ g^{-1}$. The characteristic energy (E_o), pore radius, pore volume, and average pore size are shown in Table 1.

Taking into account that they are the starting point to synthesize the biocatalysts of this work, a detailed study was carried out on the distribution of the size of the pores through the DFT; since the reports in the scientific literature are not many in this area, a comparison was made of the theoretical isotherms obtained for the NLDFT and QSDFT models for different pore shapes versus the experimental isotherms.[55] Results are shown in Table 2.

Table 2. Mean Error Adjustment between Different Surface Textures (NLDFT vs. QSDFT) in Slit and Slit/Cylindrical Pores

	NLDFT		QSDFT	
sample	fitting error (slit pore) [%]	fitting error slit-(cylindrical pore) [%]	fitting error (slit pore) [%]	fitting error slit-(cylindrical pore) [%]
MOF-199	0.60	0.14	0.84	0.70
ZIF-8	4.43	5.45	3.34	2.73

QSDFT, unlike NLDFT, is the one that best fits the experimental data of ZIF-8, possibly due to the presence of roughness and chemical and/or geometric heterogeneities in the pore wall. However, the error is large, and the theoretical isotherm has a greater dispersion, especially at low pressures (see Figure 2). This indicates that there may be more pronounced heterogeneities in the smaller pores. MOF-199 shows a good fit with a model of homogeneous pore walls by the NLDFT method.

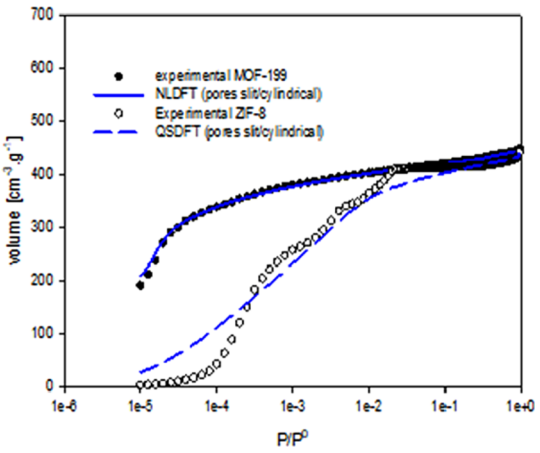

Figure 2. Analysis of the porosity by applying NLDFT and QSDFT for MOFs synthesized MOF-199/NLDFT and ZIF-8/QSDFT.

Once the most suitable model was established, the distribution of the size of the pores was studied.

As shown in Figure 3 due to the marked microporosity of the samples, the analysis of the DA equation was performed at low pressures (see Figure 4).

It can be seen that while V_{mic} presented by ZIF-8 is slightly higher than that of MOF-199 (see Table 3), the characteristic energy in the micropores is much higher in MOF-199 (this

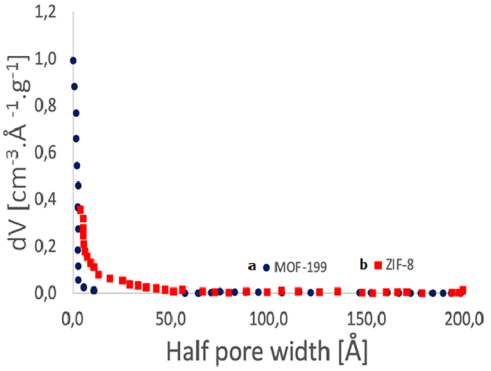

Figure 3. Porosity analysis: (a) MOF-199 (blue circles) and (b) ZIF-8 (red circles).

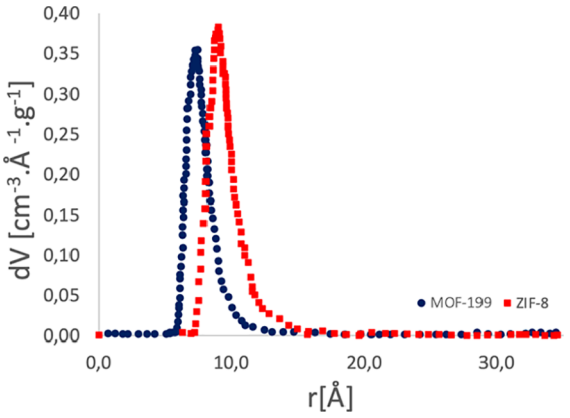

Figure 4. Size distribution of pores of MOF-199 and ZIF-8 from the N_2 adsorption isotherms at 77 K. The Weibull equation was used for the analysis of DA equation at low pressures.

surface terms the S_{BET}) and that difference a advantage N_2 adsorption.

Table 3. DA Parameters Obtained from the Adsorption Isotherm of CO_2 at 273.15 K

	DA (CO_2)			
sample	V_{mic}[$cm^3\ g^{-1}$]	E_o [Kj mol^{-1}]	N	pore radius [Å]
MOF-199	2.91	4.53	1.3	8.2
ZIF-8	5.19	1.85	1.0	10.6

The parameter n of the DA equation[54,55] provides a measure of the description of adsorption data in many microporous solids, ranging from a narrow micropore size distribution ($n \sim 3$) to a broad one ($n < 3$). In this way, and in accordance with what is observed in the graph, a narrow distribution of the size of the micropores is concluded (see $n \sim 3$ in Table 1). In order to provide more complete information in the presence of smaller micropores not detected by N_2, it is proposed to extend the investigation by adsorption of CO_2 at 273.15 K since it is sensitive to inaccessible micropores N_2 at 77 K. Adsorption equilibrium isotherms for CO_2 at 273.15 K for MOF-199 and ZIF-8 were also determined from 0 to 0.030 in relative pressure (P/P^o) in order to avoid problems caused by nitrogen. At cryogenic temperatures, allowing the adsorbate to enter the narrow microporosity,[52−55] are graphically represented in Figure 5. MOF-199 has a higher adsorption capacity compared to that of ZIF-8, probably due to morphological and chemical

https://doi.org/10.1021/acsomega.2c02873
ACS Omega 2022, 7, 41882−41904

differences. On the other hand, the narrow porosity analysis was carried out from the CO_2 isotherms (Figure 5).

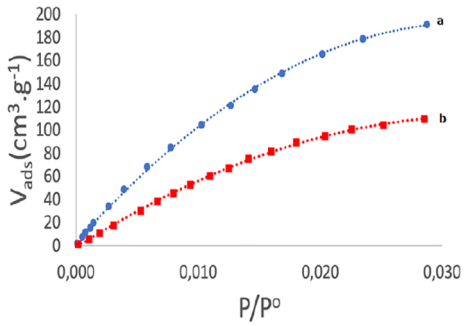

Figure 5. Adsorption−desorption isotherms of CO_2 to 273.15 K. (a) MOF-199 (blue circles) and (b) ZIF-8 (red circles).

Analysis of CO_2 adsorption data at 273.15 K using the DA equation shows that there are (closer) smaller micropores with a wide size distribution ($n < 3$). The CO_2 adsorption isotherm at 273.15 K shows that for MOF-199, the CO_2 adsorption capacity is higher, possibly associated with a higher characteristic energy in the pores. In addition, ZIF-8 shows a larger pore size distribution curve trend, indicating a greater heterogeneity (see Figure 6). It should be noted that the analysis of the adsorption

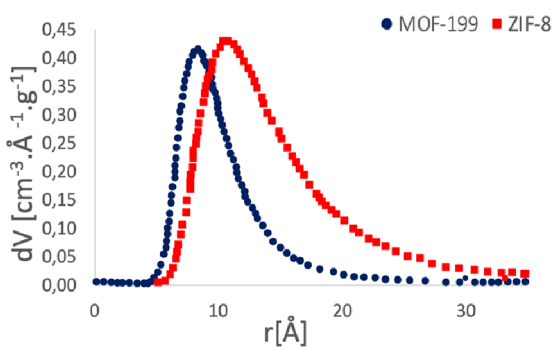

Figure 6. Size distribution of pores of MOF-199 and ZIF-8 from CO_2 adsorption isotherms at 273.15 K.

isotherms for the two MOFs used in this research study was the same as that carried out in a previous publication. The behavior of the isotherms is the same; however, here the commercial samples were used, so the textural values changed.[56]

It is interesting to note that in addition to this analysis, these MOFs used as starting materials to synthesize biocatalysts have a high CO_2 adsorption capacity. This is in good agreement with recent publications made on these materials, which show their wide spectrum of applications, especially within the area of the development of materials for the storage and separation of gases in engineering.

3.2. TG-DTA of the Starting MOF-199 and ZIF-8. The thermal behavior of the MOFs used in this research study to analyze biodiesel production (ZIF-8 and MOF-199) is shown in Figure 7. Figure 7a shows the TGA-DTA curve of MOF ZIF-8 under a nitrogen flow. The TGA curve clearly shows a long plateau up to a temperature of 420 °C, indicating a high thermal stability of the sample. Analyzing this TGA curve of ZIF-8 in detail, a small weight loss of approximately 2% around 100 °C is observed, which can be attributed to adsorbed water molecules inside the structure. Subsequently, a weight loss occurs between 450 and 600 °C, which can be attributed to the elimination of methanol from the surface and the pores of the ZIF-8 crystals, which was used during the synthesis process.

Finally, two subsequent weight losses occur at 600 °C that are associated with the decomposition of organic groups (e.g., 2-methylimidazole), which lead to the collapse of the structure.[57−69] The final weight that usually remains afterward corresponds to ZnO, which is the expected residual solid.[70−75] In summary, in a general way, we can say regarding the thermal behavior of ZIF-8 that the TGA curve exhibits a gradual weight loss step of about 20% between 450 and 600 °C, corresponding to the elimination of guest molecules (e.g., H_2O) from cavities or residual species (e.g., 2-methylimidazole) on the surface of nanocrystals.[57,73−77] After 600 °C, the TGA curve shows a steadily decreasing line indicating sample collapse.

The thermostability of MOF-199 was also investigated. A diagram corresponding to the TGA curve and the DTA of MOF-199 (Figure 7b) shows two clearly differentiated steps corresponding to the changes in weight that are associated with the structural changes that the MOF presents when under thermal analysis conditions. The first % weight loss occurred between 30 and 170 °C due to the vaporization of the present solvents used in the synthesis process ($C_2H_2Cl_2$ and DMF), which are usually occluded inside the porous structure of the MOF. The second change is a weight loss of 39.07% in the temperature range of 310−380 °C due to material decomposition. Therefore, MOF-199 is stable at temperatures up to 360 °C. Subsequently, a drastic loss of mass occurs, which is related to the decomposition of the structure in CuO.[78,79]

3.3. FTIR Analysis of the Starting MOF-199 and ZIF-8. The results corresponding to FTIR spectroscopy of the MOFs that have been used in this research study for the production of biodiesel are shown in order to analyze its purity by determining the corresponding bands reported in the specialized literature. All the vibration bands of the IR spectra (Figure 8) agreed with the published data for MOF-199 used in this work.[80,81] The IR spectra of MOF-199 exhibited the strong stretching vibration of the carboxylate anions at 1647 cm^{-1}, demonstrating the existence of the reaction of −COOH groups in 1,3,5-benzenetricarboxylic acid (BTC) with metal ions. The appearance of a broad band between 3500 and 2700 cm^{-1} indicated the presence of water and −OH groups in the structure of the material. Figure 8a shows the FTIR spectrum of ZIF-8 where the characteristic peaks at 3420 cm^{-1} and 2930 cm^{-1} are related to the aromatic and aliphatic C−H stretching of imidazole, respectively.[82,84] The absorption peak at 1591 cm^{-1} is due to C−N[84,85] stretching. The peaks at 1145 and 998 cm^{-1} correspond to C−N stretching and bending, respectively.[82−85] These characteristic peaks fully confirm the successful synthesis of ZIF-8.[85]

Figure 8b shows the FTIR spectrum corresponding to MOF-199 used in this work. The spectrum of MOF-199 is clearly dominated by a large amount of the solvent in the region of 3800−2500 cm^{-1}. In the dehydrated form, the IR absorption bands of the linker BTC are observed in the range of 1800−400 cm^{-1}.[86−88] The off-scale absorption bands in the range 1700−500 cm^{-1} and 1500−1300 cm^{-1} correspond to vasym (C−O_2) and vsym (C−O_2).[89−91] The other very intense absorption band is centered at 730 cm^{-1} and was previously assigned[86−91] to the C−H bending mode. In the considered range, only the band centered at 490 cm^{-1} is assigned to a vibrational mode that directly involves the Cu center. Following the previous

https://doi.org/10.1021/acsomega.2c02873
ACS Omega 2022, 7, 41882−41904

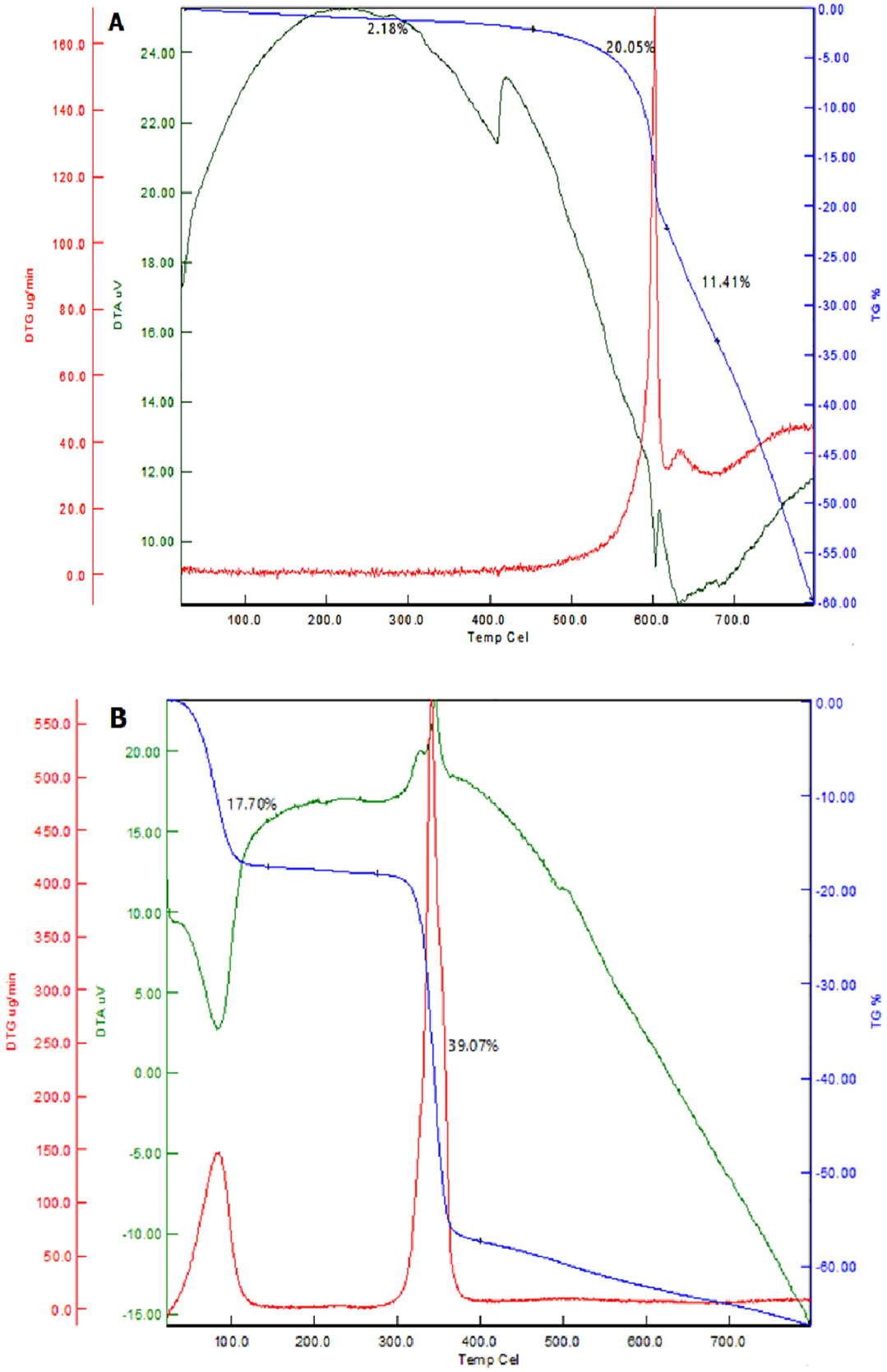

Figure 7. Thermograms of the starting MOFs: (a) ZIF-8 and (b) MOF-199.

interpretations,[88−91] this function is assigned to the Cu−O stretching mode.

3.4. SEM Analysis of the Starting MOF-199 and ZIF-8.

The morphologies of the samples are examined by SEM. The SEM image corresponding to ZIF-8 is shown in Figure 9a small

https://doi.org/10.1021/acsomega.2c02873
ACS Omega 2022, 7, 41882−41904

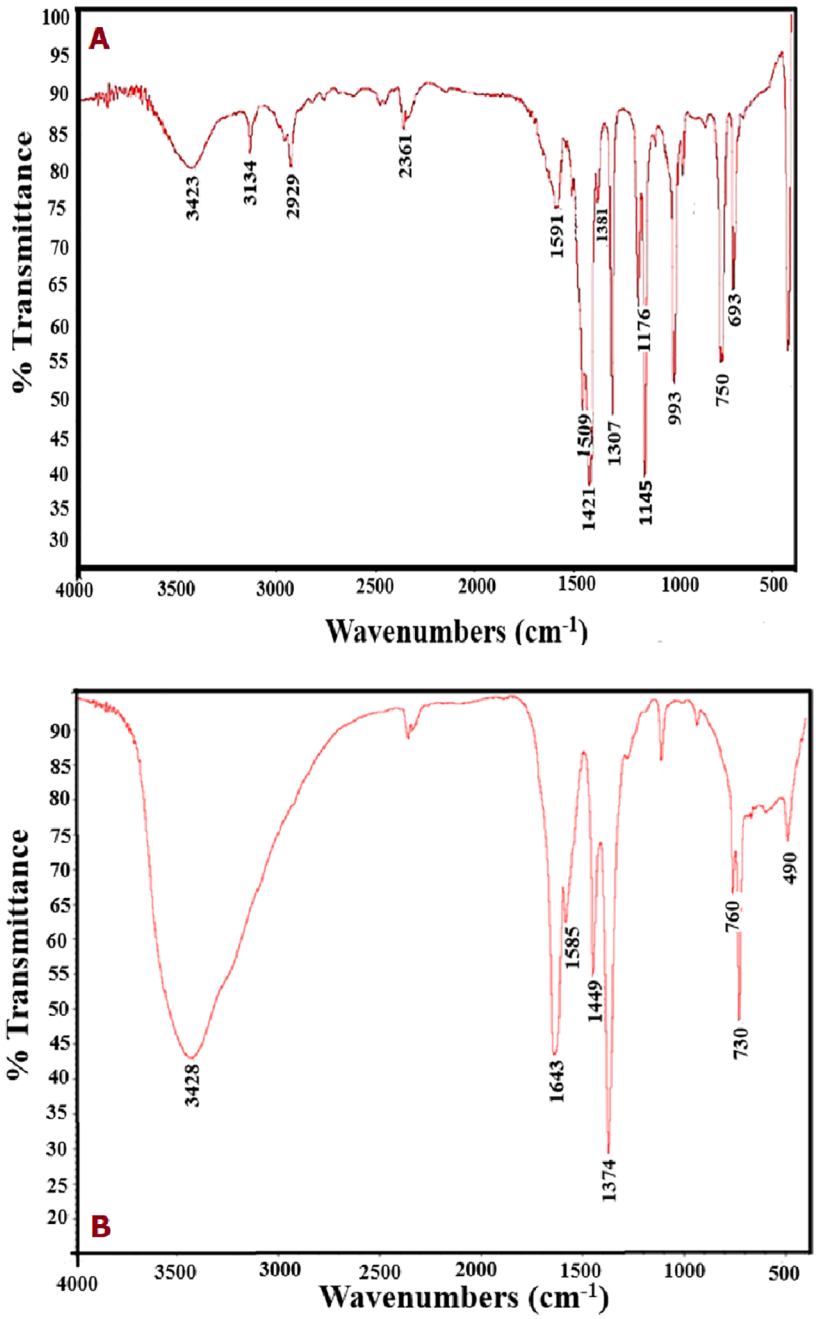

Figure 8. FTIR spectra of MOF samples used in this research study: (a) ZIF-8 and (b) MOF-199.

particles with sizes of approximately 1 μm and 0.1 μm and with shapes that vary between slightly deformed to small rhombic dodecahedrons are observed.[92−96]

The SEM image of MOF-199 is shown in Figure 9b, which is composed of polyhedral particles; the crystal structure of the MOF includes unsmoothed surfaces with obvious cracks and a porous structure that is consistent with the results reported in the literature studies.[92,96] This confirms that the samples used in this research study have a high degree of purity, a condition that is necessary for biodiesel biosynthesis tests. On the other hand, when analyzing the elemental mapping shown in Figure 10, the elemental mapping showed a homogeneous distribution of C, Zn, and N elements in ZIF-8. The O element comes from the zinc nitrate hexahydrate residue or from the conductive link used for the characterization.[93,94]

The EDS is used for elemental and chemical analyses. This analysis detects the individual elements through X-rays emitted by the materials. The energy peaks are attributed to the different elements in the sample. This analysis confirms the purity of the MOF used in this research study as observed by detecting the presence of only C, O, and Cu elements that are related to the organic ligand and the metal in the final structure of MOF-199 (Figure 11).

3.5. XRD Analysis of Unmodified MOFs Used in This Research. The XRD spectra of the two MOFs used in this investigation were examined in order to analyze their crystallinity. The XRD patterns of ZIF-8 are shown in Figure 12a. ZIF-8's XRD pattern was taken at angles from 0 to 70°. Characteristic peaks are observed between 5 and 40°. The Miller indices (h k l) for the most representative correspond to the

https://doi.org/10.1021/acsomega.2c02873
ACS Omega 2022, 7, 41882−41904

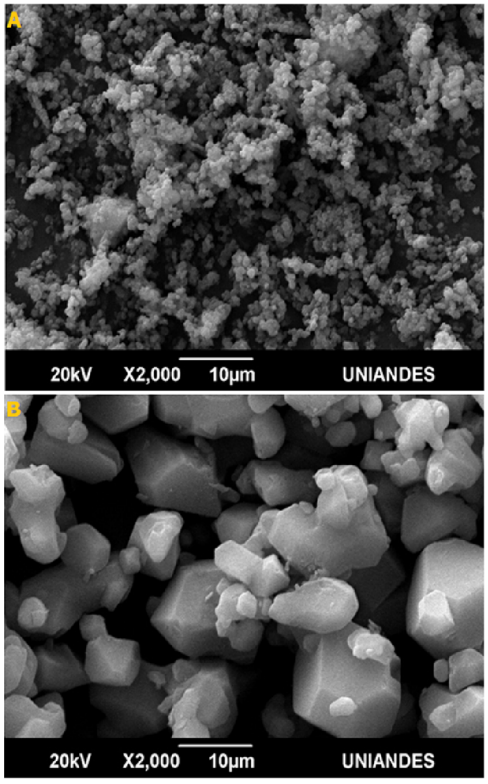

Figure 9. SEM images of used MOFs (a) ZIF-8 and (b) MOF-199.

planes (0 1 1), (0 0 2), (1 1 2), (0 2 2), (0 1 3), and (2 2 2), which shows the crystallinity of the MOFs used in this work since they coincide with those reported in the literature studies.[30,31,40,41,48,50]

The XRD pattern of MOF-199 and its Miller indices (h k l) are shown in Figure 12b. Clear and sharp peaks show the good crystallinity of the sample used. All diffraction peaks of MOF-199 agree well with the standard pattern of ZIF-8. The sample used was a pure phase of MOF-199 because no obvious impurity peaks were detected.[97,98] For this case, the difraction ray-X (DRX) corresponding to MOF-199 was also taken at angles from 0 to 70°.

Characteristic peaks are observed between 5 and 30°. By determining the Miller indices (h k l) for the most representative one, they correspond to the planes (0 1 1), (2 2 0), (0 2 2), (4 0 0), and (4 4 0), which shows likewise for this MOF its high crystallinity due to high coincidence with those reported in the literature studies.[98−102]

3.6. Biocatalyst Results: FA@MOF-199 and FA@ZIF-8. *3.6.1. Textural Characterization.* According to the procedure presented in the part of the Section 2.1.2, the starting MOFs were modified with FA. The respective N_2 isotherms at 77 K were determined to establish whether, as explained in the procedure part, the starting materials were altered. In Figure 13a, the isotherms corresponding to the materials that are now labeled FA@MOF-199 and SA@ZIF-8 are presented.

The nitrogen isotherms were measured to examine the surface area, total pore volume, and pore size distribution of FA@MOF-199 and FA@ZIF-8; the two samples show isotherms that, according to the IUPAC, belong to type IV isotherms. If they are observed carefully, at low relative pressures of N_2 due to the shape on the isotherm, it can be seen that in both samples, there are micropores, which provide, in both samples, sites that can play an important role in the subsequent use in the respective biocatalysis reactions. The N_2 adsorption isotherms present the most important result with this modification with FA result that can be seen at relatively higher pressures of P/P^o = 0.85−0.90, where in both samples, a hysteresis loop was generated, which is larger in the FA@ZIF-8 sample than in the FA@MOF-199 sample, as well as a higher nitrogen adsorption capacity.

This shows very clearly that when comparing these isotherms with those of Figure 1, corresponding to the starting samples, that the effect of FA had an effect and also that mesoporosity was generated, which is very useful in the subsequent application that is carried out will give you when you fix the lipase. When performing the respective calculations, it was determined that for sample FA@ZIF-8, its specific surface area was 787 $m^2\ g^{-1}$, while for sample FA@MOF-199, its specific area was 634 $m^2\ g^{-1}$, and the corresponding total pore volumes were 1.82 $cm^3\ g^{-1}$ for the FA@ZIF-8 sample and 1.71 $cm^3\ g^{-1}$ for the FA@MOF-199 sample. These results clearly show that the starting samples were modified by FA treatment.

In summary, after modification with FA, the final working samples to synthesize the biocatalysts present a heterogeneous distribution of pores (Figure 13b; mesopores and micropores) and some macropores. It can be inferred that during the process of obtaining the two materials, specifically by heat treatment, the structures of the MOFs were altered, especially Zn and Cu, which led to the formation of partial macropores in the samples that generate the destruction of the base structure of each sample and later, during the internal reaction processes, generated mesoporosities, which shows that the thermal treatment affected the structure additionally.[103−110] Additionally, the other analysis was carried out for these samples such as FTIR, XRD, and SEM-EDS to verify the results obtained by means of the adsorption isotherms of N_2 at 77 K. The results confirmed that the starting MOFs were indeed modified, which was especially seen with the XRD and FTIR results. In the case of the XRD results, in both samples, the peaks between 25 and 45 (in the 2θ range) decrease radically, verifying the effect of the addition of FA. While for the FTIR those presented in the starting MOFs in the range in addition to the FTIR, they showed that FA did insert into the structures of the MOFs, since the two FTIR of the starting samples were also modified in the zone of the region of 3500 cm^{-1} generated a string band to the vibration of the −OH of FA, and in the area between 1500 and 750 cm^{-1}, new strong and well-defined bands were seen that correspond to the different groups and vibrations of FA. We have not presented each of the results here due to lack of space and additionally because they will be a part of another publication.

3.6.2. Study of the Optimal Conditions to Fix PCL and Obtain Biocatalysts FA@MOF-199-PCL and FA@ZIF-8-PCL. Prior to the preparation of the biocatalysts (FA@MOF-199-LPC and FA@ZIF-8-PLC), it is recommended to establish the optional conditions to achieve the best immobilization of lipase on the different supports because these parameters have effects evident on not only the immobilization but also the % yield in the production of green biodiesel and its specific activity. That is why this part of the research studied the (1) enzyme load, (2) enzyme immobilization time, (3) enzyme immobilization temperature, and (4) the effect of pH on the % immobilization of the enzyme and the specific activity. For this, the enzyme (PCL) was loaded between 1.0 and 6.0 mg/mg of FA@MOF-199 and FA@ZIF-8, respectively. Figure 14a shows that the highest immobilization efficiency for the FA@ZIF-8 support had a value of 91.2% when the load was 3.5 mg/mg of this support and had a specific activity of 142.5 U/g protein. The FA@ZIF-8

https://doi.org/10.1021/acsomega.2c02873
ACS Omega 2022, 7, 41882−41904

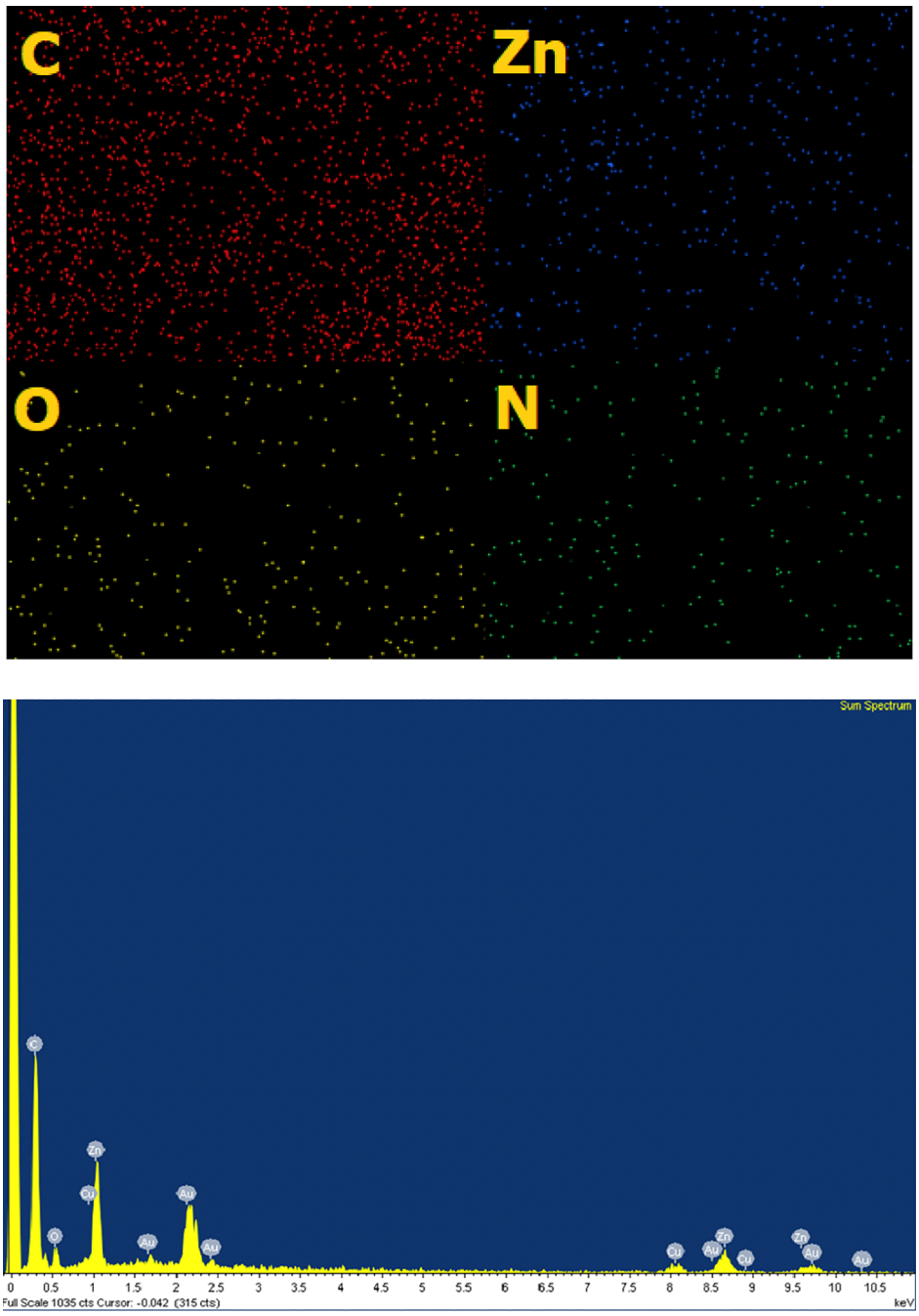

Figure 10. Elemental mapping of ZIF-8.

support presented 80.3% enzyme immobilization and 125% U/g protein specific activity.[111−122] From these results, it was determined that 3.5 mg/mg would be used as a load for the preparation of the biocatalysts as an enzyme load for both supports as an adequate enzymatic load for subsequent studies. As shown in Figure 14b, the specific activity increases in the period from 0.5 to 5.0 h for all three systems tested. After this time, both the specific activity and the enzyme immobilization efficiency decrease.[116−120] In this assay, FA@ZIF-8-PCL presents 95% efficiency in the immobilization of the enzyme and 149 U/g protein of specific activity, being the highest of the three. Therefore, 5.0 h (immobilization efficiency of 95 and 85% for FA@MOF-8 and FA@MOF-199, respectively) was chosen as the most appropriate time for PCL immobilization.[122] The effect of temperature as a function of immobilization between 10 and 70 °C was also investigated. The immobilization efficiency increased slowly for both supports as the immobilization temperature increased over the range of 20−40 °C. Beyond this temperature, the specific activity of the immobilized lipase and the recovery of activity began to decrease (Figure 14c). Therefore, in this work, 40 °C was set as the optimal immobilization temperature.[122]

On the other hand, the pH value of the medium is an important factor to achieve an adequate immobilization of the enzyme. Figure 14d shows that a neutral environment is beneficial for the immobilization of PCL on the synthesized supports. The maximum activity reached its value of 125.4 and 110.3 U/g protein for FA@ZIF-8 and FA@MOF-199 when the

https://doi.org/10.1021/acsomega.2c02873
ACS Omega 2022, 7, 41882−41904

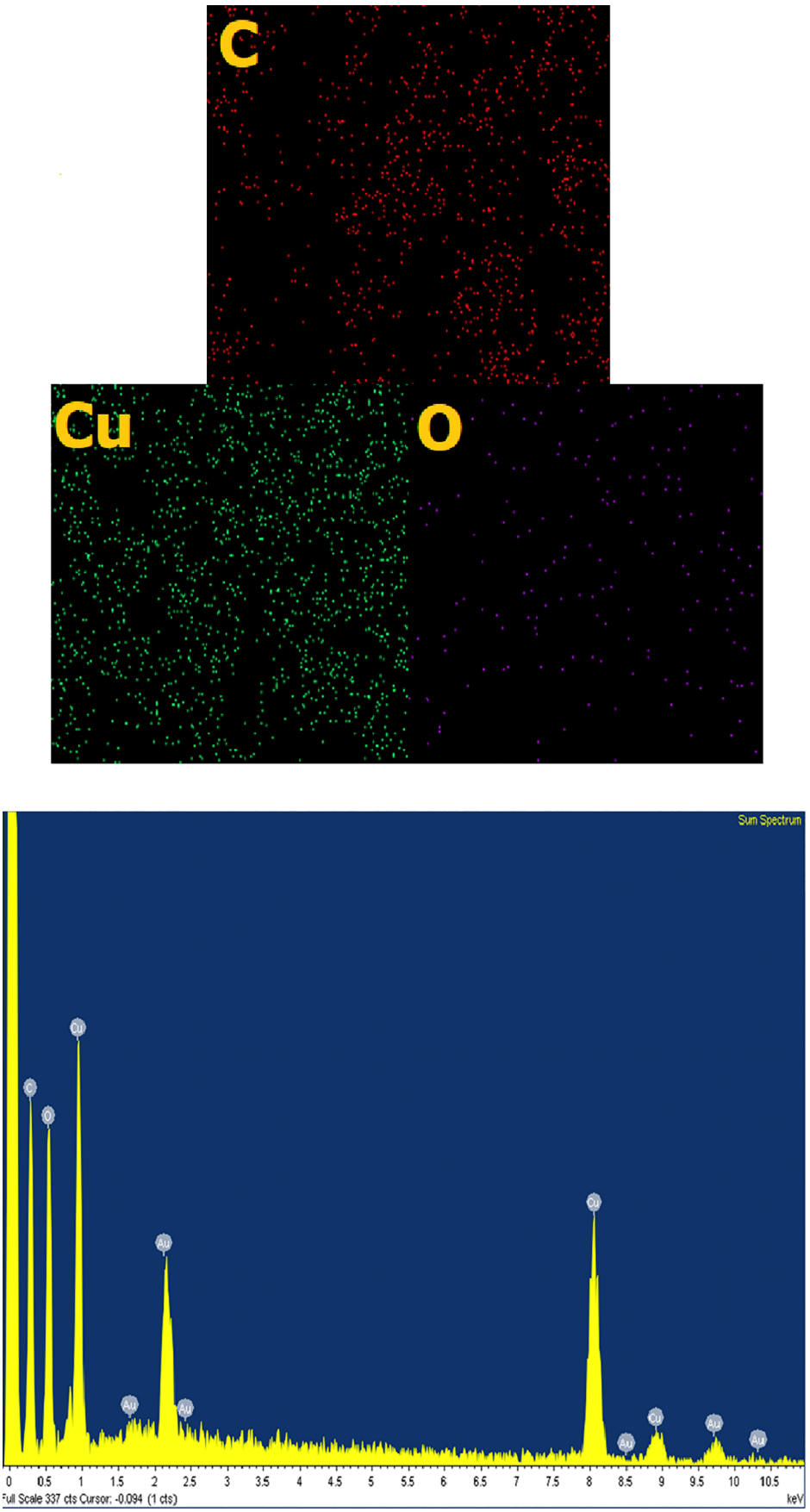

Figure 11. Elemental mapping of MOF-199.

https://doi.org/10.1021/acsomega.2c02873
ACS Omega 2022, 7, 41882−41904

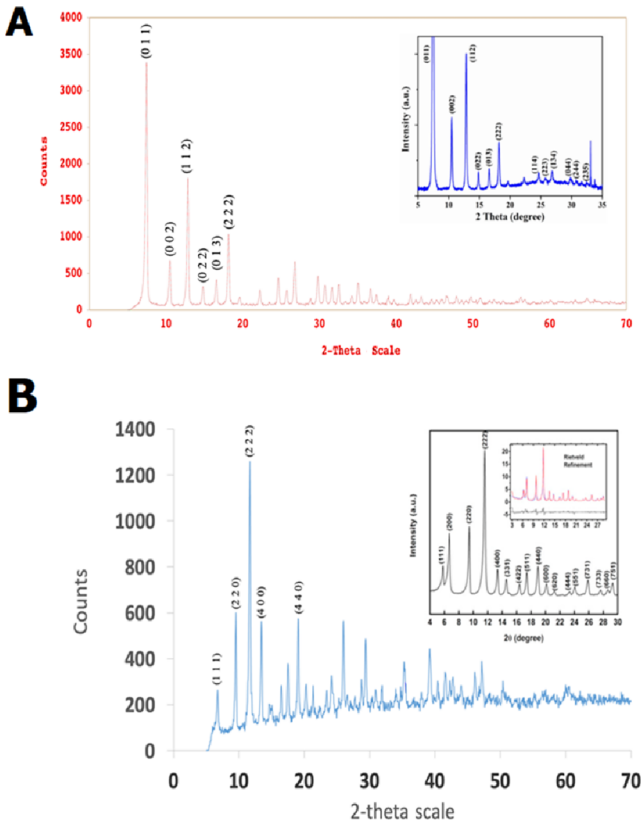

Figure 12. XRD patterns of (a) ZIF-8 and (b) MOF-199. The XRD patterns in the insets are the XRD patterns reported in the literature.

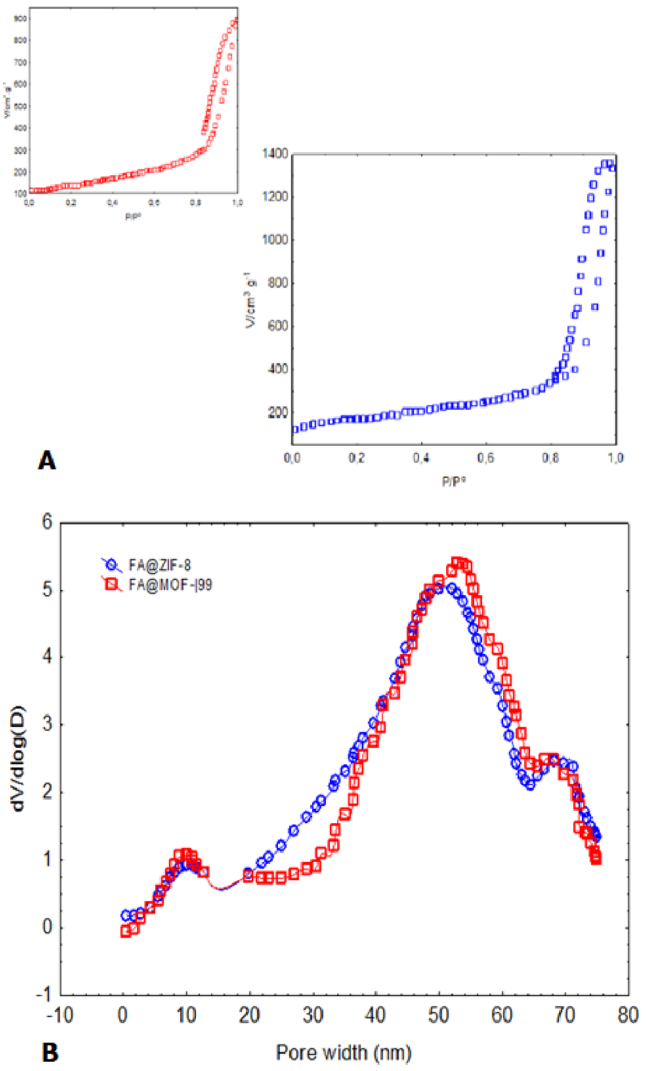

Figure 13. (a) Nitrogen adsorption−desorption isotherms (red: FA@MOF-199; blue: FA@ZIF-8) and (b) pore size distribution.

pH of the buffer was 7.0. The immobilization efficiency changed slightly after pH 8.0, where lipase is probably denatured at the pH values. Thus, phosphate buffer was used in all the immobilization processes with the highest recovery of activity at pH 7.0.[115−125,122] Therefore, the maximum recovery of specific activity was 125.4 U/g protein for FA@ZIF-8 and 110.3 U/g protein for FA@MOF-199 under immobilization conditions optimized by a factor: enzyme load = 3.5 mg/mg of supports, immobilization time = 5.0 h for both supports, immobilization temperature = 40 °C, and phosphate buffer at pH 7.0.[121,122]

3.5.3. Synthesis of Biodiesel under Optimal Pre-established Conditions and Study of Biocatalysts Based on the Methanol Molar Ratio, Oil, Temperature, Dosage, and Reaction Time. Finally, the biocatalysts synthesized in this work (FA-@MOF-199-PCL and FA@ZIF-8-PCL) were taken and used to carry out the transesterification of APO in a methanolic medium. To set PCL, the previously established parameters were used, and the performance of the synthesized biodiesel was studied based on the effect of (1) the molar ratio of methanol:oil and the method of addition, (2) the temperature, (3) the dosage of the biocatalysts, and (4) the reaction time, and subsequently, the results were analyzed. The results obtained in this research study show a high yield during the synthesis of biodiesel using PCL immobilized on the two biocatalysts prepared in this work under the experimental conditional previously established in this research, showing a high catalytic activity.

Analyzing the results in detail, and in particular the studies on the effect of biodiesel production depending on the dosage of methanol during the chemical reaction under study, and taking into account that there are not enough exhaustive studies that address investigations of the effect of the dosage of methanol to the system of the transesterification reaction of oils and fats to obtain biodiesel, that is, if there is any difference when it is added in a single step to the reaction system or in several. In this work, this type of study is addressed, where we base ourselves on research reported in the scientific literature, where the authors found that there was an effect and therefore, we wanted to verify if it was fulfilled for our systems.[122−125] Figure 15a shows the effect that different molar ratios of methanol:palm oil have on the transesterification reaction and the method of addition of methanol in biodiesel production using free lipase and FA@ZIF-8 and its influence on the yield of biodiesel production in the same time intervals (only the results with the FA@ZIF-8@PCL biocatalyst are shown here).

In this investigation, the methanol addition methods employed were as follows: (1) methanol was added in a single step, (2) methanol was added in two steps with an interval of 3 h; (3) methanol was added in three steps at 3 h intervals; and (4) methanol was added in four steps at 3 h intervals. The results show that despite there being differences, these are very small between the three- and four-step methanol addition methods. When using the three- and four-step methanol addition methods, the biodiesel yield was greater than 90% for the

https://doi.org/10.1021/acsomega.2c02873
ACS Omega 2022, 7, 41882−41904

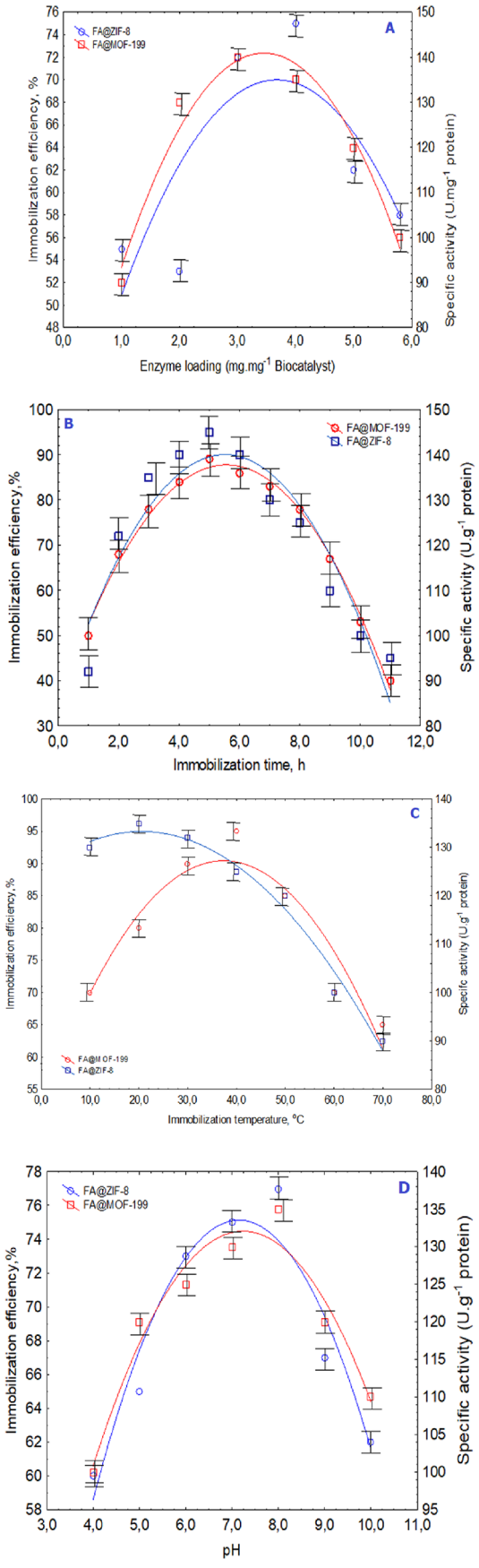

Figure 14. Effect of different immobilizations on specific efficiency. (a) Effect of enzyme loading, (b) effect of immobilization, (c) effect of immobilization temperature, and (d) effect of pH value. The standard deviation (SD) is represented by error bars at a confidence level of 95% in the figure.

Figure 14. continued

biocatalysts synthesized in this work (FA@ZIF-8-PCL and FA@MOF-199-PCL) and above 70% for free PCL, and the maximum yield was reached at a molar ratio of methanol:APO of 1 when using the one-step method under the same reaction conditions (as mentioned above). Only the results of FA@ZIF-8-PCL are presented here; however, it should be noted that the results for biocatalyst FA@MOF-199-PCL and lipase-free PCLpresented the same behavior). On the other hand, it can be seen in Figure 15b that the maximum yield of biodiesel increases for the three systems used in transesterification, in which it reached its maximum value at a molar ratio of methanol:palm oil of 4:1 for all the steps used. For the addition of methanol. However, the results show that the molar ratio and the system used to add methanol have a drastic influence on the yield during the synthesis of biodiesel from APO and that under the conditions of this experiment and in particular with the biocatalysts used, the procedure of adding methanol to the system is very important. It has been shown for this particular system that between three- and four-step methods, there is a significant difference in the yield of green biodiesel.

This result shows that it is important to address this type of difference because, according to the systems used, the yield of the transesterification reaction can be improved. Finally, it should be noted that despite the fact that free PCL generated a good performance, when supported on catalysts modified with FA, its power of action on the components of APO is much higher, and this is a novel aspect. Studies with the varying temperature for FA@ZIF-8-PCL, FA@MOF-199-PCL, and free PCL show that as the system is placed at a higher temperature, the reaction is faster and ultimately generates a higher yield of biodiesel.

This is the result of a clearly kinetic aspect where, as the temperature increases, the oil molecules move faster toward the catalyst, which in turn manages to reduce the kinetic energy; however, when it is desired to fix the reaction temperature, care must be taken because lipase can denature if brought to extreme temperatures. The results shown in Figure 15c (performed at a 4:1 methanol:oil ratio and using the three-step method regarding the addition of methanol) allow us to deduce that the biodiesel yield increases slowly when the reaction temperature is gradually increased in the interval from 10 °C to 30 °C; FA@ZIF-8-PCL again has the best yield, followed by FA@ZIF-8-PCL, and finally free FA@MOF-199-PCL. Although lipase shows good yields in the production of biodiesel, clearly, when it is supported on catalysts modified with FA, its yield drastically improves.

After 30 °C, the yield of biodiesel production decreases for the case of FA@ZIF-PCL and free lipase, while for FA@MOF-199-PCL, it remained constant. This study concluded that the optimum reaction temperature was 30 °C with biodiesel yields of 95, 90, and 83% for FA@ZIF-8-PCL, FA@MOF-199-PCL, and free PCL, respectively.

Results of the transesterification reaction of palm oil as a function of time are shown in Figure 15d for FA@ZIF-8-PCL, FA@MOF-PCL, and free PCL, using a 4:1 molar ratio. (methanol:oil), adding methanol in three steps and at 30 °C. The results obtained are very interesting and show that the biocatalyst reaches a yield of 100% after 8 h of reaction, while

https://doi.org/10.1021/acsomega.2c02873
ACS Omega 2022, 7, 41882−41904

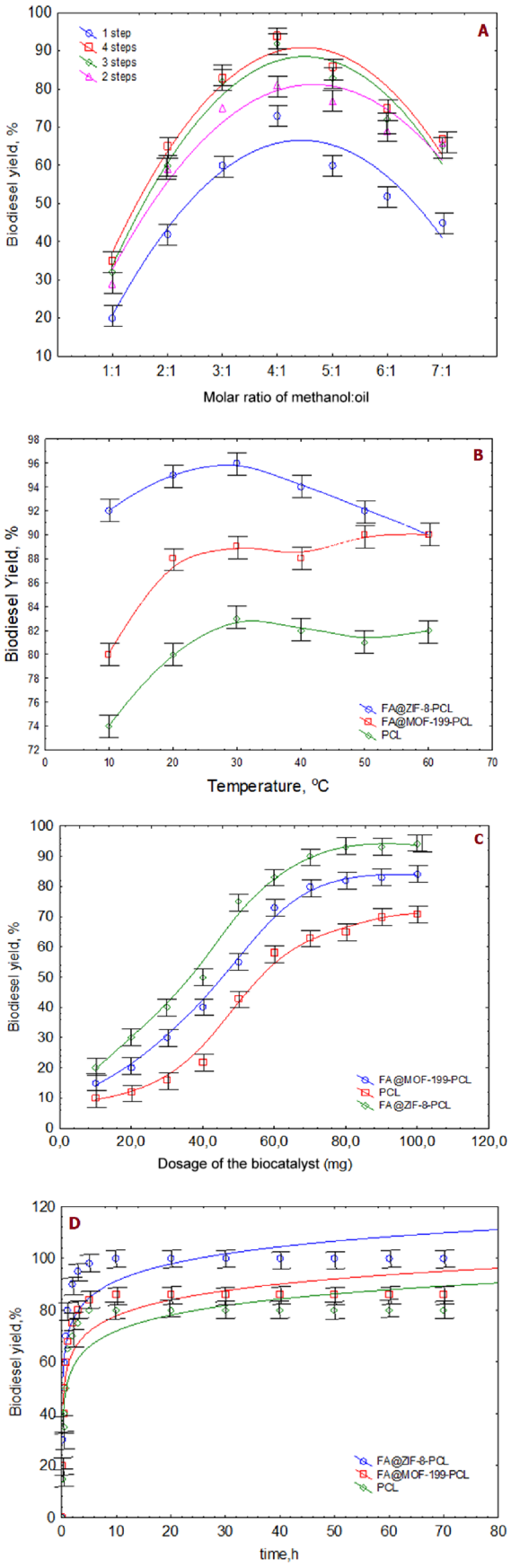

Figure 15. Yield of synthesized biodiesel under different conditions: (a) methanol:oil molar ratio and addition method; (b) temperature; (c) dosage of the biocatalysts; and (d) reaction time. The SD is represented by error bars at a confidence level of 95% in the figure.

Figure 15. continued

FA@MOF-199-PCL reaches a yield of 85% and free PCL reaches 80%. In any case, the three systems present promising yields, but the excellent yield of the biocatalysts synthesized in this work is worth highlighting.

Finally, a study of biodiesel yield was carried out based on the dosage of biocatalysts and free PCL, using a molar ratio of 4:1 (methanol:oil), adding methanol in three steps, at 30 °C and setting the reaction time to 8 h.

Figure 15e shows the results for this experiment, and the results are very interesting: what stands out for the three systems is the sigmoidal behavior of the curves, which reach a maximum value of biodiesel of 905, 80, and 70% for FA@ZIF-8-PCL, FA@MOF-PCL, and free PCL, respectively. The results show that dosages of 70 mg of the catalyst of free PCL generate the maximum yield in biodiesel production under the conditions of this investigation.

It is interesting to perform this type of statistical calculations basically on the main parameters that influence the transesterification reaction of APO. The parameters considered were the reaction temperature, methanol:oil ratio, reaction time, and biocatalyst dosage. Taking into account that the optimization designs are time-consuming, a Taguchi L9 orthogonal array (OA) was used, where the four optimizable parameters can each accommodate three levels. A mathematical analysis of variance (ANOVA) was used to assess the reliability of the results and statistical significance. The *p*-values for the four variables analyzed lie between 0.0113 and 0.010, showing a low probability of error. During the research, some parameters were evaluated statistically using ANOVA to analyze the reliability of the methodology used in this work.

Several tests were performed on sum of squares (SS) values according to which the parametric contribution to performance is evaluated: Fischer's exact test values (*F*-value) which measure the statistical significance of data points through the analysis of their distribution in the multivariate matrix (L9) and the deviation from a null hypothesis, as well as error probability values (*p*-value) which are a measure of the *F*-value obtained as a result of chance. It is known that high *F*-values indicate stability of the experimental method in this case and of the factor and are associated with a low *p*-value (<0.05 essential), which indicates a low probability of errors (only the relevant results are mentioned, taking into account that the statistical part here is only an instrument).

In this investigation, the biocatalysts presented SS values of 102.14 and 189.34, with *F*-values of 37.43 and 453.43 for FA@ZIF-8-PCL and FA@ZIF-8-PCL and with *p*-values of 0.019 and 0.0010, respectively. Furthermore, according to the results obtained, the mathematical model was adjusted to minimize all the data points, and it was also evaluated if it presents any "residual" for the biocatalysts synthesized in this work.

3.5.4. Physical and Chemical Properties of APO and Synthesized Biodiesel. The detailed physicochemical characteristics of the starting palm oil and the biodiesel synthesized in this investigation were determined and are listed in Table 4. The kinematic viscosity of the biodiesel produced is comparable to the standard values of the ASTM D6751 standard;[126−130] the acid value of the biodiesel was found to be 0.350 mg KOH g^{-1} and that of APO was 0.645 mg KOH g^{-1}, while the calorific value

https://doi.org/10.1021/acsomega.2c02873
ACS Omega 2022, 7, 41882−41904

Table 4. Comparison of the Physicochemical Properties of APO and Its Biodiesel Derivative by FA@ZIF-8-PCL Using EN and ASTM Standards

		biodiesel		biodiesel B100				
		FA@ZIF-8-PCL (ASTM)	FA@ZIF-8-PCL (EN)	EN		ASTM		
property	APO	this work	this work	min	max	min	max	references
density (kg m^3)	865	880	870	860	900	820	880	134,135
humidity (mg kg^{-1})	298	350	158		500		500	135
acid value (mgKOH g^{-1})	0.645	0.350	0.27		0.50			136
saponification index (mg KOH g^{-1})	189.45	192.50				189.00	198.00	137
viscosity (at 40 °C, mm^2 s^{-1})	43.2	4.86	4.43	3.5	5.0	1.9	6.0	134,135
centane number	17.3	49.5	52.5	51		40		135
calorific value (MJ kg^{-1})	21.43	37.89	41.2	35		35	.	136
flash point (°C)		145.50	110	101		130	170	135

of biodiesel was 37.89 MJ Kg^{-1} (Table 4) and that of APO was 21.43 MJ Kg^{-1}. The flash point is an important parameter that must be considered during the storage of any (flammable) liquid fuel. The flash point of the biodiesel was 145.50 °C, a value that is within the range according to the recommendations of the ASTM D975 standard. The values of the physicochemical characteristics obtained in this work are fundamentally due to the composition of those of APO and biodiesel.[125−132] However, the values are within the standards established by the ASTM, so the green biodiesel obtained by means of the biocatalysts synthesized in this research is of good quality.[126−130]

3.5.5. Analysis of Biodiesel with FTIR Spectroscopy and GC−MS Using the FA@ZIF-8-PCL Biocatalyst. It is important to analyze the biodiesel samples obtained through the transesterification of APO in order to verify that the reaction took place. Here, we only present FTIR and GC−mass spectroscopy GC−MS results that show that the reaction did indeed occur. The FTIR and GC−MS analyses are shown, corresponding to the biodiesel obtained with the FA@ZIF-8-PCL biocatalyst.

In the FTIR spectra of the crude APO used as the starting raw material to perform transesterification and obtain the biodiesel with the biocatalysts prepared in this research produced presented in Figure 16a as well as the FT-IR of the biodiesel obtained.

When performing the analysis of each of the FTIR bands corresponding to the APO, the most characteristic ones are found, among which those that show the presence of symmetric C−H bonds around 2800 and 3000 cm^{-1}. The band that is around 2922 cm^{-1} is assigned to vegetable oils; some authors also assign it to biodiesel to the vibrations of the methyl groups, and finally, a band can also be seen at 1743 cm^{-1} that corresponds to the divisions and vibrations of acid esters and fatty esters. The differences between both spectra are the intensity in the aforementioned peaks.

The FTIR spectrum of the biodiesel synthesized using the FA@ZIF-8-PCL biocatalyst obtained from crude APO shows a signal that is not completely resolved toward 1200 cm^{-1} assigned to the axial deformation of CC(=O)−O, which is assigned to the bond vibrations attributed to ester bonds. A signal around 1170 cm^{-1} appears in the FTIR spectrum of biodiesel, which some researchers assign to an asymmetric deformation of O−C−C bonds. The FTIR spectrum exhibits a zone corresponding to the functional groups of 1750−1740 cm^{-1}; it has an intense peak corresponding to the carbonyl group (C=0). According to the transesterification reaction, for each methyl ester formed, there is a transformation from a $-CH_2$ group to a $-CH_3$ group,[131] which in Figure 16a is identified by the difference between the intensities of 2922 and 1170 cm^{-1} in both spectra, as has been widely discussed by other authors.[132] While for APO, the difference between both signals is not noticeable, in biodiesel, it is more significant, as is the signal at 1170 cm^{-1}.[133] These results are shown in Table 4; these, together with the other results obtained in this research study, allow us to demonstrate that good-quality biodiesel was synthesized.

Figure 16b shows one of the chromatograms taken from the biodiesel samples synthesized in this work. The gas chromatogram shown corresponds to a biodiesel sample obtained with the FA@ZIF-8-PCL biocatalyst, which presents the characteristic peaks of a biodiesel sample reported in the literature. GC analysis showed that the main FAMEs present (and their composition) were as follows: C12:0 (0.35%), C14:0 (1.15%), C16:0 (44.25%), C16:1 (0.21%), C18:0 (4.45%), C18:1 (42.20%), C18:2 (6.67%), C18:3 (0.52%), and C20:0 (0.20%). Because the polarity of the column used was very high, here, it is observed that it eludes C20:0 (arachidic) before C18:3 (linolenic), which is in very good agreement with that reported by the literature.[134] As is common in this type of biofuels synthesized from APO, palmitic acid (44.25%) and oleic acid (42.20%) are the ones with the highest percentage. This demonstrates that the biocatalysts work by carrying out the transesterification of APO.

4. DISCUSSION AND ANALYSIS

When comparing the textural characteristics of the starting materials with those of the biocatalysts, it is noteworthy (Tables 5 and 6) that the total volume increased for both ZIF-8 and MOF-199 when modified with furfuryl acid. This increase in volume is due to the fact that when FA is coupled to the MOF network, it creates new pores. The size of these new pores depends on the interaction of FA with the support. In the case of the interaction of ZIF-8 with FA, for the formation of these new pores, it must be taken into account that furfuryl acid is structurally formed by a furanyl group and a hydroxymethyl group; the furanyl group presents electronic resonance as does the imidazolate anion, but due to the high electronic density, these two groups cannot form a pi-stacking system; therefore, FA cannot be anchored in this way to ZIF-8. The hydroxymethyl group of furfuryl acid via the hydroxyl group can easily interact with the basic nitrogens of the imidazolate group by forming hydrogen bridges; however, the nitrogen atoms of the imidazolate anion are bonded to zinc atoms in the MOF structure which does not allow this type of interaction. As the imidazolate anions are electronically resonant, the medium is

https://doi.org/10.1021/acsomega.2c02873
ACS Omega 2022, 7, 41882−41904

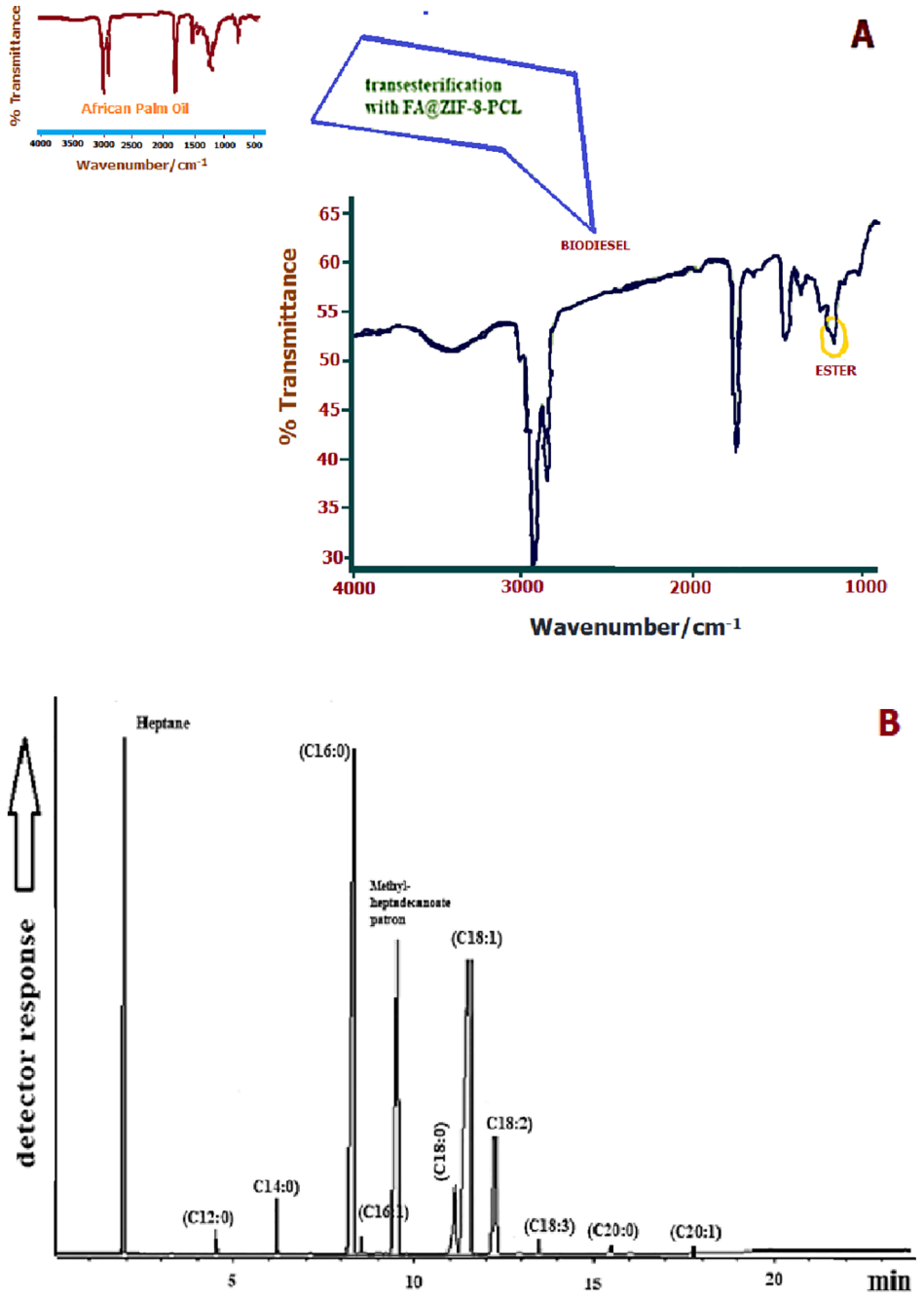

Figure 16. (a) FTIR spectra of APO and the biodiesel product of transesterification using biocatalyst FA@ZIF-8-PCL. (b) Gas chromatograph of the biodiesel synthesized from APO using biocatalyst FA@ZIF-8-PCL.

Table 5. Improved Textural Properties by the Use of FA to Modify ZIF-8

	materials					
			STA/ZIF8			
properties	ZIF-8	FA@ZIF-8	10% STA	20% STA	30% STA	ZIF-8/pluronic P123
superficial area ($m^2\ g^{-1}$)	1750	787	877.2	995.9	1088.1	1610
total volume ($cm^3\ g^{-1}$)	0.88	1.82	0.59	0.54	0.47	0.73
references	this investigation	140	141			

maintained at pH 7, and FA has a pKa between 15 and 16,[138] and the hydrogens present in the hydroxyl groups of FA can form hydrogen bridges with the pi-cloud of the imidazolate group without any problem (see Scheme 1); this interaction is responsible for the formation of new pores with a larger pore volume. The change in pore volume from 0.88 to 1.82 $cm^3\ g^{-1}$ from ZIF-8 to FA@ZIF-8 facilitates the anchoring of *PCL* because the furanyl groups with a high electron density are more exposed relative to the imidazolate groups. This increased exposure allows a better interaction between the hydrophobic

https://doi.org/10.1021/acsomega.2c02873
ACS Omega 2022, 7, 41882−41904

Table 6. Improved Textural Properties by the Use of FA to Modify MOF-199

	materials							
			GO/MOF-199			TEA/MOF-199		
properties	MOF-199	FA@MOF-199	0.5% GO	1.75% GO	5% GO	n = 1	n = 2	n = 3
superficial area ($m^2\ g^{-1}$)	1733	634	684.971	777.88	684.894	550	187	25
total volume ($cm^3\ g^{-1}$)	0.66	1.71	1.024	1.1897	1.026	0.21	0.07	0.01
references	this investigation	142	143					

Scheme 1. Hydrogen Bond between FA and the Electron Cloud of the Ligand in the MOF Structure: Most Probable Interaction

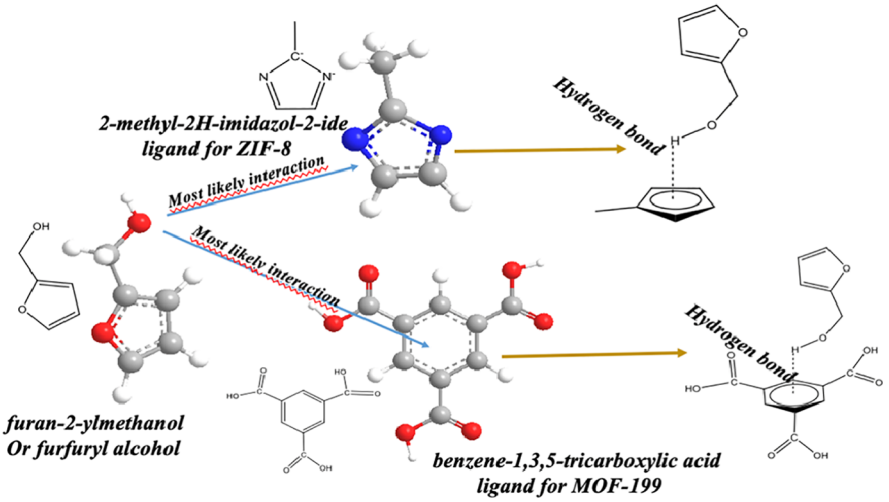

amino acids of *PCL*, which have a high acidity for high-electron-density groups,[139] resulting in a better immobilization and higher thermal resistance of the new catalytic material compared to that with free lipases. The use of FA enlarges the pores of the modified ZIF-8 to a greater extent compared to the use of other modifiers such as silico-tungstic acid (in different percentages) and Pluronic P123 copolymer (see Table 5); additionally, it improves the textural properties that allow better anchoring of *PCL*. Regarding the interaction of MOF-199 with FA, it is noteworthy that the pore volume change from 0.66 to 1.71 $cm^3\ g^{-1}$ improves the anchoring capacity of *PCL*in a similar way to that of ZIF-8, with the difference that BTC is the ligand that allows the anchoring of FA to the MOF-199 structure, which binds to the Cu atoms by the three carboxylate groups. Therefore, the only interaction option with FA is by the formation of hydrogen bridges with the new electron of the phenyl group ligand of MOF-199 and with the hydrogens of the hydroxyl group of FA; we recognize that a pi-stacking system between the phenyl group of BTC and the furanyl group of FA cannot be formed due to their high electronic densities. The above corresponds to the explanation why the immobilization of *PCL* on FA@MOF-199 was less strong than the immobilization of *PCL* on FA@ZIF-8; additionally, it should be considered that the phenyl ring generates greater steric hindrance because it is larger than the five-carbon ring of the imidazolate group of ZIF-8.

The use of FA for the modification of MOF-199 is motivated by the fact that the use of other modifiers such as GO and tertiary amine triethanolamine (TEA), it is evident that FA enlarges the pores of the modified MOF-199 to a greater extent and improves the textural properties of the new biocatalyst in relation to these two types of catalysts and the starting material (see Table 6), which allows better anchoring of *PCL*.

Regarding the synthesis of biodiesel from the FA@ZIF-8 and FA@MOF-199 biocatalysts, it should be noted that the biodiesel components derived from the acylglycerides present in AFO are within the ranges required by the EN and the ASTM standards as required by the European Union (EU).

Table 4 shows that this work was carried out for the synthesis of green biodiesel. The results in Section 3.2.2 show that the performance of the biocatalysts follows the following order: FA@ZIF-8 > FA@MOF-199 > PCL-Free; this behavior can be explained as follows: although in both catalysts FA@ZIF-8 and FA@MOF-199, the furanyl groups of FA are oriented perpendicular to their anchoring point on the imidazolate groups and the phenyl groups on ZIF-8 and MOF-199, respectively (see Scheme 1), the distances between and angles of separation of the furanyl groups are different.

For FA@ZIF-8, the angle of inclination is greater than the separation distance between one group and the other, generating a cone-shaped inclination between the furanyl groups, a configuration conferred by the methyl groups adjacent to the imidazolate groups, whereas in FA@MOF-199, the configuration of the furan groups is not much conical, but their distribution tends to be a mixture of semiconical and parallel because the phenyl groups of BTC are symmetrically distributed around the phenyl groups. The cone shape acquired by FA when anchored to the electron cloud of the imidazolate anion on FA@ZIF-8 allows better anchoring of *PCL* and enables this biocatalyst to exhibit greater stability and therefore higher yields. The higher yield achieved by the FA@ZIF-8-PCL and FA@MOF-199-PCL biocatalysts compared to that by PCL-free demonstrates that the use of FA as a modifier is a novel aspect in the conversion of palm oil into biodiesel components.

https://doi.org/10.1021/acsomega.2c02873
ACS Omega 2022, 7, 41882−41904

5. CONCLUSIONS

In this research, two biocatalysts have been prepared from MOF-199 and ZIF-8, modified with FA, and adsorbed on *PCL*to perform the synthesis of biodiesel from APO. The results showed that the two biocatalysts prepared in this research show yields greater than 90% in their biodiesel synthesis capacity, higher than those of the catalysts reported in the specialized literature. Additionally, in this study, it is shown that it is necessary to control variables such as temperature, pH, lipase dosage, and lipase immobilization time, which are important in the control for the adequate fixation on lipase and its subsequent and adequate functioning. Finally, the effect on the yield of the methanol:oil molar ratio and the way of adding methanol to the reaction system, temperature, and reaction time were studied in this work.

AUTHOR INFORMATION

Corresponding Author

Juan Carlos Moreno-Piraján − *Facultad de Ciencias, Departamento de Química, Grupo de Investigación en Sólidos Porosos y Calorimetría, Universidad de los Andes, Bogotá 01, Colombia;* orcid.org/0000-0001-9880-4696; Email: jumoreno@uniandes.edu.co

Authors

José Manuel Martínez Gil − *Grupo de Investigación Catálisis y Materiales. Facultad de Ciencias Básicas y Aplicadas, Universidad de La Guajira, Riohacha 440007, Colombia; Grupo de Investigación Química Cuántica y Teórica, Facultad de Ciencias Exactas y Naturales, Universidad de Cartagena, Cartagena 130005, Colombia; Grupo de Investigación Desarrollo de Estudios y Tecnologías Ambientales del Carbono (DESTACAR). Facultad de Ingenierías, Universidad de La Guajira, Riohacha 440007, Colombia; Facultad de Ciencias, Departamento de Química, Grupo de Investigación en Sólidos Porosos y Calorimetría, Universidad de los Andes, Bogotá 01, Colombia*

Ricardo Vivas Reyes − *Grupo de Investigación Química Cuántica y Teórica, Facultad de Ciencias Exactas y Naturales, Universidad de Cartagena, Cartagena 130005, Colombia;* orcid.org/0000-0002-7462-1948

Marlon Bastidas-Barranco − *Grupo de Investigación Desarrollo de Estudios y Tecnologías Ambientales del Carbono (DESTACAR). Facultad de Ingenierías, Universidad de La Guajira, Riohacha 440007, Colombia*

Liliana Giraldo − *Facultad de Ciencias, Departamento de Química, Grupo de Calorimetría, Universidad Nacional de Colombia, Sede Bogotá 01, Colombia*

Complete contact information is available at: https://pubs.acs.org/10.1021/acsomega.2c02873

Notes

The authors declare no competing financial interest.

ACKNOWLEDGMENTS

The authors thank the framework agreement between the Universidad Nacional de Colombia and Universidad de los Andes (Bogotá, Colombia) under which this work was carried out. Professor J.C.M.-P.á also thanks for an award from the Facultad de Ciencias of Universidad de los Andes, number INV-2021-128−2257, and the support from "Publica tus Nuevos Conocimientos y Expón tu Nuevas Creaciones", de la Vicerrectoría de investigaciones de la Universidad de los Andes (Bogotá, Colombia).

REFERENCES

(1) Diniz, A. P. M. M.; Sargeant, R.; Millar, G. J. Stochastic techno-economic analysis of the production of aviation biofuel from oilseeds. *Biotechnol. Biofuels* **2018**, *11*, 161.

(2) Kumar, K.; Thakur, S. T.Biodiesel production from trans-esterification of Serratia sp. ISTD04 lipids using immobilised lipase on biocomposite materials of biomineralized products of carbon dioxide sequestrating bacterium, *Bioresour. Technol.*, **2020**, *307*, 123193, ISSN 0960-8524, pp 845−856, DOI: 10.1016/j.biortech.2020.123193.

(3) Shah, S.; Sharma, S.; Gupta, M. N. Biodiesel Preparation by Lipase Catalyzed. *Transesterification of Jatropha Oil, Energy & Fuels* **2004**, *18*, 154−159.

(4) Sakdasri, W.; Sawangkeaw, R.; Ngamprasertsith, S. Techno-economic analysis of biodiesel production from palm oil with supercritical methanol at a low molar ratio. *Energy* **2018**, *152*, 144−153.

(5) Pikula, K. S.; Zakharenko, A. M.; Chaika, V. V.; Stratidakis, A. K.; Kokkinakis, M.; Waissi, G.; Rakitskii, V. N.; Sarigiannis, D. A.; Hayes, A. W.; Coleman, M. D.; Tsatsakis, A.; Golokhvast, K. S. Toxicity bioassay of waste cooking oil-based biodiesel on marine microalgae. *Toxicol. Rep.* **2019**, *6*, 111−117.

(6) Roy, M. M.; Wang, W.; Bujold, J. Biodiesel production and comparison of emissions of a DI diesel engine fueled by biodiesel−diesel and canola oil−diesel blends at high idling operations. *Appl. Energy* **2013**, *106*, 198−208.

(7) Abed, K. A.; Gad, M. S.; El Morsi, A. K.; Sayed, M. M.; Elyazeed, S. Effect of biodiesel fuels on diesel engine emissions. *Egypt. J. Pet.* **2019**, *28*, 183−188.

(8) Ajala, O. E.; Aberuagba, F.; Odetoye, T. E.; Ajala, A. M. Biodiesel: sustainable energy replacement to petroleum-based diesel fuel − a review. *Chem. Biol. Eng. Rev* **2015**, *2*, 145−156.

(9) Bhatia, S. K.; Kim, J.; Song, H.; Kim, H. J.; Jeon, J.; Sathiyanarayanan, G.; Yoon, J.; Park, K.; Kim, Y.; Yang, Y. Microbial biodiesel production from oil palm biomass hydrolysate using marine Rhodococcus sp. *YHY01. Biores. Technol* **2017**, *233*, 99−109.

(10) Thliveros, P.; Uçkun Kiran, E. U.; Webb, C. Microbial biodiesel production by direct me- thanolysis of oleaginous biomass. *Biores. Technol* **2014**, *157*, 181−187.

(11) Martinez-Silveira, A.; Villarreal, R.; Garmendia, G.; Rufo, C.; Vero, S. Process conditions for a rapid in situ transesterification for biodiesel production from oleaginous yeasts. *Electron. J. Biotechnol* **2019**, *38*, 1−9.

(12) Su, F.; Guo, Y. Advancements in solid acid catalysts for biodiesel production. *Green Chem.* **2014**, *16*, 2934−2957.

(13) Thangaraj, B.; Solomon, P. R.; Muniyandi, B.; Ranganathan, S.; Lin, L. Catalysis in biodiesel production—a review. *Clean Energy* **2019**, *3*, 2−23.

(14) de Lima, A. L.; Ronconi, C. M.; Mota, C. J. A. Heterogeneous basic catalysts for biodiesel production. *Catal. Sci. Technol.* **2016**, *6*, 2877−2891.

(15) Borges, M. E.; Díaz, L. Recent developments on heterogeneous catalysts for bio- diesel production by oil esterification and trans-esterification reactions: a review. *Renew. Sustain. Energy Rev* **2012**, *16*, 2839−2849.

(16) Melero, J. A.; Iglesias, J.; Morales, G. Heterogeneous acid catalysts for biodiesel production: current status and future challenges. *Green Chem.* **2009**, *11*, 1285−1308.

(17) Arumugam, A.; Ponnusami, V. Production of biodiesel by enzymatic transester- ification of waste sardine oil and evaluation of its engine performance. *Heliyon* **2017**, *3*, No. e00486.

(18) Ha, S. H.; Lan, M. N.; Lee, S. H.; Hwang, S. M.; Koo, Y.-M. Lipase-catalyzed biodiesel production from soybean oil in ionic liquids. *Enzy. Microbial Technol* **2007**, *41*, 480−483.

(19) Sahu, G. K.; Martin, M. Optimization of growth conditions for the production of extracellular lipase by bacterial strains from dairy industry effluents. *Biotechnol. Bioinf. Bioeng* **2011**, *1*, 305−311.

(20) Bueso, F.; Moreno, L.; Cedeño, M.; Manzanarez, K. Lipase-catalyzed biodiesel production and quality with Jatropha curcas oil: exploring its potential for Central America. *J. Biol. Eng* **2015**, *9*, 12.
(21) Amini, Z.; Ilham, Z.; Ong, H. C.; Mazaheri, H.; Chen, W.-H. State of the art and prospective of lipase-catalyzed transesterification reaction for biodiesel production. *Energy Convers. Manage.* **2017**, *141*, 339−353.
(22) Mu, Y.; Xiu, Z.-L.; Zhang, D.-J. A combined bioprocess of biodiesel production by lipase with microbial production of 1,3-propanediol by Klebsiella pneumoniae. *Biochem. Eng. J.* **2008**, *40*, 537−541.
(23) Rana, Q.; Laiq Ur Rehman, M.; Ahmed, M.; Hasan, S.; Shah, F.; Khan, A. A.; Badshah, S.; Badshah, M. Lipolytic bacterial strains mediated transesterification of non- edible plant oils for generation of high-quality biodiesel. *J. Biosci. Bioeng.* **2019**, *127*, 609−617.
(24) Zhang, B.; Weng, Y.; Xu, H.; Mao, Z. Enzyme immobilization for biodiesel production. *Appl. Microbiol. Biotechnol.* **2012**, *93*, 61−70.
(25) Andrade, T. A.; Martín, M.; Errico, M.; Christensen, K. V. Biodiesel production catalyzed by liquid and immobilized enzymes: optimization and economic analysis. *Chem. Eng. ResDesign* **2019**, *141*, 1−14 ISSN 0263-8762.
(26) Li, L.; Dyer, P. W.; Greenwell, H. C. Biodiesel production via trans-esterification using Pseudomonas cepacia immobilized on cellulosic polyurethane. *ACS Omega* **2018**, *3*, 6804−6811.
(27) Singh, J.; Singh, M.; Kumar, I. S.; Thakur, I. S. Immobilized lipase from Schizophyllum commune ISTL04 for the production of fatty acid methyl ester from cynobacterial oil. *Biores. Technol* **2015**, *188*, 214−218.
(28) Alamsyah, G.; Albels, V. A.; Sahlan, M.; Hermansyah, H. Effect of chitosan's amino group in adsorption-crosslinking immobilization of lipase enzyme on resin to catalyze biodiesel synthesis. *Energy Proc* **2017**, *136*, 47−52.
(29) Xie, W.; Huang, M. Immobilization of Candida rugosa lipase onto graphene oxide Fe_3O_4 nanocomposite: characterization and application for biodiesel production. *Energy Convers. Manage.* **2018**, *159*, 42−53.
(30) El-Batal, A. I.; Farrag, A. A.; Elsayed, M. A.; El-Khawaga, A. M. Biodiesel production by Aspergillus niger lipase immobilized on barium ferrite magnetic nanoparticles. *Bioengineering* **2016**, *3*, 14.
(31) Patel, S. K. S.; Choi, S. H.; Kang, Y. C.; Lee, J. K. Eco-friendly composite of Fe3O4-reduced graphene oxide particles for efficient enzyme immobilization. *ACS Appl. Mater. Interfaces* **2017**, *9*, 2213−2222.
(32) Babaki, M.; Yousefi, M.; Habibi, Z.; Mohammadi, M.; Yousefi, P.; Mohammadi, J. Enzymatic production of biodiesel using lipases immobilized on silica nanoparticles as highly reusable biocatalysts: effect of water, t-butanol and blue silica gel contents. *Renewable Energy* **2016**, *91*, 196−206.
(33) Gao, Y.; Tan, T.-W.; Nie, K.-L.; Wang, F. Immobilization of lipase on macroporous resin and its application in synthesis of biodiesel in low aqueous media. *Chin. J. Biotechnol* **2006**, *22*, 114−118.
(34) Macario, A.; Moliner, M.; Diaz, U.; Jorda, J. L.; Corma, A.; Giordano, G. Biodiesel production by immobilized lipase on zeolites and related materials. *Stud. Surf. Sci. Catalysis* **2008**, *174*, 1011−1016.
(35) Ou, J.; Yuan, X.; Liu, L.; Zhang, P.; Xu, W.; Tang, K.Lipase from Pseudomonas cepacia immobilized into ZIF-8 as biocatalyst for enantioselective hydrolysis and transesterification, Process Biochem. **2021**, *102*, 132−140, ISSN 1359-5113, DOI: 10.1016/j.procbio.2020.12.017.
(36) Qiu, X.; Zhong, W.; Bai, C.; Li, Y. Encapsulation of a metal-organic polyhedral in the pores of a metal-organic framework. *J. Am. ChemSoc* **2016**, *138*, 1138−1141.
(37) Shen, K.; Zhang, L.; Chen, X.; Liu, L.; Zhang, D.; Han, Y.; Chen, J.; Long, J.; Luque, R.; Li, Y.; Chen, B. Ordered macro-microporous metal-organic framework single crystals. *Science* **2018**, *359*, 206−210.
(38) Zhou, X. W.; Huang, J.; Shi, Z.; Zhao, Q.; Xia, Y.; Li, H.; Wang, Z.; Li, Z. A novel MOF/graphene oxide composite GrO@MIL-101 with high adsorption capacity for acetone. *J. Mater. Chem.* **2014**, *2*, 4722−4730.
(39) Gong, Q.; Hu, Z.; Deibert, B. J.; Emge, T. J.; Teat, S. J.; Banerjee, D.; Mussman, B.; Rudd, N. D.; Li, J. Solution processable MOF yellow phosphor with exceptionally high quantum efficiency. *J. Am. Chem. Soc.* **2014**, *136*, 16724−16727.
(40) Yao, J.; Liu, Y.; Wang, J.; Jiang, Q.; She, D.; Guo, H.; Sun, N.; Pang, Z.; Deng, C.; Yang, W.; Shen, S. On-demand CO release for amplification of chemotherapy by MOF functionalized magnetic carbon nanoparticles with NIR irradiation. *Biomaterials* **2019**, *195*, 51−62.
(41) Yasutaka, K.; Takato, Y.; Takashi, K.; Kohsuke, M.; Hiromi, Y. Enhancement in adsorption and catalytic activity of enzymes immobilized on phosphorus- and calcium-modified MCM-41. *Phys. Rev. B: Condens. Matter Mater. Phys.* **2011**, *115*, 10335−10345.
(42) He, H.; Han, H.; Shi, H.; Tian, Y.; Sun, F.; Song, Y.; Li, Q.; Zhu, G. Construction of thermophilic lipase-embedded metal-organic frameworks via biomimetic mineralization: a biocatalyst for ester hydrolysis and kinetic resolution. *ACS Appl. Mater. Interfaces* **2016**, *8*, 24517−24524.
(43) Niknam Shahrak, M.; Ghahramaninezhad, M.; Eydifarash, M. Zeolitic imidazolate framework-8 for efficient adsorption and removal of Cr(VI) ions from aqueous solution. *Environ. Sci. Pollut. Res.* **2017**, *24*, 9624−9634.
(44) Lykourinou, V.; Chen, Y.; Wang, X.-S.; Meng, L.; Hoang, T.; Ming, L.-J.; Musselman, R. L.; Ma, S. Immobilization of MP-11 into a mesoporous metal-organic framework, MP-11@mesoMOF: a new platform for enzymatic catalysis. *J. Am. Chem. Soc.* **2011**, *133*, 10382−10385.
(45) Zhao, S.; Zhang, Y.; Wu, Y.; Zhang, L. H.; Hu, L.; Jin, L. ZIF-derived hierarchical pore carbons as high-performance catalyst for methane decomposition. *J. Energy Inst.* **2022**, *100*, 197−205.
(46) Thommes, M.; Cychosz, K. A.; Neimark, A. V.*Advanced physical adsorption characterization of nanoporous carbons*. In *Novels Carbons Adsorbent*; Tascón, J. M. D., Ed.; Elsevier: Great Britain, 2012. Corpus ID: 15168106, 107-145.
(47) Rouquerol, J.; Llewellyn, P.; Rouquerol, F.*Is the bet equation applicable to microporous adsorbents?*. In *Characterization of porous solids VII*; Lewellyn, P., Rodríguez-Reinoso, F., Rouquerol, J., Seaton, N., Eds.; Elsevier, Stud. Surf. Sci. Catal: Amsterdam, 2007; Vol. *160*, pp 49−56.,
(48) Chen, R.; Yao, J.; Gu, Q.; Smeets, S.; Baerlocher, C.; Gu, H.; Zhu, D.; Morris, W.; Yaghi, O. M.; Wang, H. A. Two-dimensional zeolitic imidazolate framework with a cushion-shaped cavity for CO_2 adsorption. *Chem. Commun.* **2013**, *49*, 9500−9502.
(49) Fairen-Jimenez, D.; Moggach, S. A.; Wharmby, M. T.; Wright, P. A.; Parsons, S.; Düren, T. Opening the gate: Framework Flexibility in ZIF-8 Explored by Experiments and Simulations. *J. Am. Chem. Soc.* **2011**, *133*, 8900−8902.
(50) Danaci, D.; Singh, R.; Xiao, P.; Webley, P. A. Assessment of ZIF materials for CO_2 capture from high pressure natural gas streams. *Chem. Eng. J.* **2015**, *280*, 486−493.
(51) Garrido, J.; Linares-Solano, A.; Martin-Martinez, J. M.; Molina-Sabio, M.; Rodriguez-Reinoso, F.; Torregrosa, R. Use of nitrogen vs. Carbón dioxide in the characterization of activated carbons. *Langmuir* **1987**, *3*, 76−81.
(52) Brunauer, S.; Emmett, P. H.; Teller, E. Adsorption of gases in multimolecular layers. *J. Am. Chem. Soc.* **1938**, *60*, 309−319.
(53) Landers, J.; Gor, G. Y.; Neimark, A. V. Density functional theory methods for characterization of porous materials. *Colloids Surf., A: Physicochemical and Eng. Aspects* **2013**, *437*, 3−32.
(54) Dubinin, M. M.; Astakhov, V. A. Development of the Concepts of Volume Filling of Micropores in the Adsorption of Gases and Vapors by Microporous Adsorbents. *Russ. Chem. Bull.* **1971**, *20*, 3−7.
(55) Li, G.; Lan, J.; Liu, J.; Jiang, G. Synergistic adsorption of As(V) from aqueous solution onto mesoporous silica decorated orderly with Al2O3 and Fe_2O_3 nanoparticles. *J. Colloid Interface Sci.* **2013**, *405*, 164−170.
(56) Giraldo, L.; Bastidas-Barranco, M.; Húmpola, P.; Moreno-Piraján, J. C. Design, synthesis and characterization of MOF-199 and

https://doi.org/10.1021/acsomega.2c02873
ACS Omega 2022, 7, 41882−41904

ZIF-8: Applications in the adsorption of phenol derivatives in aqueous solution. *Eur. J. Chem.* **2017**, *8*, 293−304.
(57) Zhao, X.; Fang, X.; Wu, B.; Zheng, S.; Zheng, N. Facile synthesis of size-tunable ZIF-8 nanocrystals using reverse micelles as nano-reactors. *Sci. China: Chem.* **2014**, *57*, 141−146.
(58) Phan, A.; Doonan, CJ.; Uribe-Romo, FJ.; Knobler, CB.; O'Keeffe, M.; Yaghi, O. M. Synthesis, structure, and carbon dioxide capture properties of zeolitic imidazolate frameworks. *Acc. Chem. Res.* **2010**, *43*, 58−67.
(59) Demessence, A.; Boissière, C.; Grosso, D.; Horcajada, P.; Serre, C.; Férey, G.; Soler-Illia, G. J. A. A.; Sanchez, C. Adsorption properties in high optical quality nanoZIF-8 thin films with tunable thickness. *J. Mater. Chem.* **2010**, *20*, 7676−7681.
(60) Wang, B.; Côté, A. P.; Furukawa, H.; O'Keeffe, M.; Yaghi, O. M. Colossal cages in zeolitic imidazolate frameworks as selective carbon dioxide reservoirs. *Nature* **2008**, *453*, 207−211.
(61) Li, L. M.; Wang, H. F.; Yan, X. P. Metal-organic framework ZIF-8 nanocrystals as pseudo-stationary phase for capillary electrokinetic chromatography. *Electrophoresis* **2012**, *33*, 2896−2902.
(62) Chang, N.; Gu, Z. Y.; Yan, X. P. Zeolitic imidazolate framework-8 nanocrystal coated capillary for molecular sieving of branched alkanes from linear alkanes along with high-resolution chromatographic separation of linear alkanes. *J. Am. Chem. Soc.* **2010**, *132*, 13645−13647.
(63) Jiang, H. L.; Liu, B.; Akita, T.; Haruta, M.; Sakurai, H.; Xu, Q. Au@ZIF-8: CO oxidation over gold nanoparticles deposited to metal-organic framework. *J. Am. Chem. Soc.* **2009**, *131*, 11302−11303.
(64) Zhu, M. Q.; Srinivas, D.; Bhogeswararao, S.; Ratnasamy, P.; Carreon, M. A. Catalytic activity of ZIF-8 in the synthesis of styrene carbonate from CO_2 and styrene oxide. *Catal. Commun.* **2013**, *32*, 36−40.
(65) Lu, G.; Li, S.; Guo, Z.; Farha, O. K.; Hauser, B. G.; Qi, X.; Wang, Y.; Wang, X.; Han, S.; Liu, X.; DuChene, J. S.; Zhang, H.; Zhang, Q.; Chen, X.; Ma, J.; Loo, S. C.; Wei, W. D.; Yang, Y.; Hupp, J. T.; Huo, F. W. Imparting functionality to a metal-organic framework material by controlled nanoparticle encapsulation. *Nat. Chem.* **2012**, *4*, 310−316.
(66) Karagiaridi, O.; Lalonde, M. B.; Bury, W.; Sarjeant, A. A.; Farha, O. K.; Hupp, J. T. Opening ZIF-8A catalytically active zeolitic imidazolate frame-work of sodalite topology with unsubstituted linkers. *J. Am. Chem. Soc.* **2012**, *134*, 18790−18796.
(67) Dang, T. T.; Zhu, Y.; Ngiam, J. S. Y.; Ghosh, S. C.; Chen, A.; Seayad, A. M. Palladium nanoparticles supported on ZIF-8 as an efficient heterogeneous catalyst for aminocarbonylation. *ACS Catal.* **2013**, *3*, 1406−1410.
(68) Kuo, C. H.; Tang, Y.; Chou, L. Y.; Sneed, B. T.; Brodsky, C. N. Z.; Zhao, C. K.; Tsung, C.-K. Yolk-shell nanocrystal@ZIF-8 nanostructures for gas-phase heterogeneous catalysis with selectivity control. *J. Am. Chem. Soc.* **2012**, *134*, 14345−14348.
(69) Li, Z.; Zeng, H. C. Surface and bulk integrations of single-layered Au or Ag nanoparticles onto designated crystal planes {110} or {100} of ZIF-8. *Chem. Mater.* **2013**, *25*, 1761−1768.
(70) Torad, N. L.; Hu, M.; Kamachi, Y.; Takai, K.; Imura, M.; Naito, M.; Yamauchi, Y. Facile synthesis of nanoporous carbons with controlled particle sizes by direct carbonization of monodispersed ZIF-8 crystals. *Chem. Commun.* **2013**, *49*, 2521−2523.
(71) Chaikittisilp, W.; Hu, M.; Wang, H.; Huang, H. S.; Fujita, T.; Wu, K. C.; Chen, L. C.; Yamauchi, Y.; Ariga, K. Nanoporous carbons through direct carbonization of a zeolitic imidazolate framework for supercapacitor electrodes. *Chem. Commun.* **2012**, *48*, 7259−7726.
(72) Wang, Q.; Xia, W.; Guo, W.; An, L.; Xia, D.; Zou, R. Functional zeolitic-imidazolate-framework-templated porous carbon materials for CO capture and enhanced capacitors. *Chem Asian J* **2013**, *8*, 1879−1885.
(73) Lu, G.; Hupp, J. T. Metal-organic frameworks as sensors: A ZIF-8 based Fabry-Perot device as a selective sensor for chemical vapors and gases. *J. Am. Chem. Soc.* **2010**, *132*, 7832−7833.
(74) Kreno, L. E.; Leong, K.; Farha, O. K.; Allendorf, M.; Van Duyne, R. P.; Hupp, J. T. Metal-organic framework materials as chemical sensors. *Chem. Rev.* **2012**, *112*, 1105−1125.
(75) Liu, S.; Xiang, Z. H.; Hu, Z.; Zheng, X. P.; Cao, D. P. Zeolitic imidazolate framework-8 as a luminescent material for the sensing of metal ions and small molecules. *J. Mater. Chem.* **2011**, *21*, 6649−6653.
(76) Lin, W.; Rieter, W. J.; Taylor, K. M. Modular synthesis of functional nano- scale coordination polymers. *Angew Chem Int Ed* **2009**, *48*, 650−658.
(77) Miralda, C. M.; Macias, E. E.; Zhu, M.; Ratnasamy, P.; Carreon, M. A. Zeolitic imidazole framework-8 catalysts in the conversion of CO_2 to chloropropene carbonate. *ACS Catal.* **2012**, *2*, 180−183.
(78) Pan, Y. C.; Liu, Y. Y.; Zeng, G. F.; Zhao, L.; Lai, Z. P. Rapid synthesis of zeolitic imidazolate framework-8 (ZIF-8) nanocrystals in an aqueous system. *Chem. Commun.* **2011**, *47*, 2071−2073.
(79) Blanco-Brieva, G.; Campos-Martin, J. M.; Al-Zahrani, S. M.; Fierro, J. L. Thermal regeneration of the metal organic frameworks used in the adsorption of refractory organosulfur compounds from liquid fuels. *Fuel* **2013**, *105*, 459−465.
(80) Ethiraj, A.; Bonino, F.; Lamberti, C.; Bordiga, S. H2S interaction with HKUST-1 and ZIF-8 MOFs: A multitechnique study. *Microporous Mesoporous Mater.* **2015**, *207*, 90−94.
(81) Li, Y.; Yang, R. T. Hydrogen storage in metal-organic and covalent-organic frameworks by spillover. *AIChE J.* **2008**, *54*, 269−279.
(82) Thi, T. V. N.; Luu, C. L.; Hoang, T. C.; Nguyen, T.; Bui, T. H.; Nguyen, P. H. D.; Thi, T. P. P. Synthesis of MOF-199 and application to CO2 adsorption. *Adv. Nat. Sci.: Nanosci. Nanotechnol.* **2013**, *4*, 035016.
(83) Khajavian, M.; Salehi, E.; Vatanpour, V. Nanofiltration of dye solution using chitosan/poly(vinyl alcohol)/ZIF-8 thin film composite adsorptive membranes with PVDF membrane beneath as support, Carbohydr. *Polym* **2020**, *247*, 116693.
(84) Wu, C. H.; Xie, D. G.; Mei, Y. J.; Xiu, Z. F.; Poduska, K. M.; Li, D. C.; Xu, B.; Sun, D. F. Unveiling the thermolysis natures of ZIF-8 and ZIF-67 by employing in situ structural characterization studies. *Phys. Chem. Chem. Phys.* **2019**, *21*, 17571−17577.
(85) Yahia, M.; Phan Le, Q. N. P.; Ismail, N.; Essalhi, M.; Sundman, O.; Rahimpour, A.; Dal-Cin, M. M.; Tavajohi, N. Effect of incorporating different ZIF-8 crystal sizes in the polymer of intrinsic microporosity, PIM-1, for CO_2/CH_4 separation. *Microporous Mesoporous Mater* **2021**, *312*, 110761.
(86) Ren, B. H.; Chen, Y. N.; Li, Y. Q.; Li, W. J.; Gao, S. Y.; Li, H. F.; Cao, R. Rational design of metallic anti-corrosion coatings based on zinc gluconate@ZIF-8. *Chem. Eng. J.* **2020**, *384*, 123389.
(87) Prestipino, C.; Regli, L.; Vitillo, J. G.; Bonino, F. A.; Damin, C.; Lamberti, A.; Zecchina, P. L.; Solari, K. O.; Kongshaug, S.; Bordiga, S. Local structure of framework Cu (II) in HKUST1 metal-organic framework: spectroscopic characterization upon activation and interaction with adsorbate. *Chem. Mater.* **2006**, *18*, 1337−1346.
(88) Bordiga, S.; Regli, L.; Bonino, F.; Groppo, E.; Lamberti, C.; Xiao, B.; Wheatley, P. S.; Morris, R. E.; Zecchina, A. Adsorption properties of HKUST-1 toward hydrogen and other small molecules monitored by IR. *Phys. Chem. Chem. Phys.* **2007**, *9*, 2676−2685.
(89) Lin, K. S.; Adhikari, A. K.; Ku, C. N.; Chiang, C. L.; Kuo, H. Synthesis and characterization of porous HKUST-1 metal organic frameworks for hydrogen storage. *Int. J. Hydrogen Energy* **2012**, *37*, 13865−13871.
(90) Borfecchia, E.; Maurelli, S.; Gianolio, D.; Groppo, E.; Chiesa, M.; Bonino, F.; Lamberti, C. Insights into adsorption of NH3 on HKUST-1 metal−organic framework: a multitechnique approach. *J. Phys. Chem. C* **2012**, *116*, 19839−19850.
(91) Li, H.; Feng, X.; Guo, Y.; Chen, D.; Li, R.; Ren, X.; Jiang, X.; Dong, Y.; Wang, B. A malonitrile-functionalized metal-organic framework for hydrogen sulfide detection and selective amino acid molecular recognition. *Sci. Rep.* **2014**, *4*, 4366.
(92) Ethiraj, A.; Bonino, F.; Lamberti, C.; Bordiga, S. H2S interaction with HKUST-1 and ZIF-8 MOFs: A multitechnique study. *Microporous Mesoporous Mater.* **2015**, *207*, 90−94.
(93) Kida, K.; Okita, O.; Fujita, F.; Tanaka, T.; Miyake, M. Formation of high crystalline ZIF-8 in an aqueous solution. *CrystEngComm* **2013**, *15*, 1794−1801.

https://doi.org/10.1021/acsomega.2c02873
ACS Omega 2022, 7, 41882−41904

(94) Jian, M.; Liu, B.; Liu, R.; Qu, J.; Wang, H.; Zhang, X. Water-based synthesis of zeolitic imidazolate framework-8 with high morphology level at room temperature. *RSC Adv.* **2015**, *5*, 48433−48441.
(95) Tanaka, T.; Kida, K.; Okita, O.; Ito, I.; Miyake, M. Size-controlled synthesis of zeolitic imidazolate framework-8 (ZIF- 8) crystals in an aqueous system at room temperature. *Chem. Lett.* **2012**, *41*, 1337−1339.
(96) Cravillon, J. S. S.-J. A. K. M.; Münzer, S.; Lohmeier, S.-J.; Feldhoff, A.; Huber, K.; Wiebcke, M. Rapid room-temperature synthesis and characterization of nanocrystals of a prototypical zeolitic imidazolate framework. *Chem. Mater.Chemistry of Materials* **2009**, *21*, 1410−1412.
(97) Zhang, H.; Shi, Q.; Kang, X.; Dong, J. Vapor-assisted conversion synthesis of prototypical zeolitic imidazolate framework-8. *J. Coord. Chem.* **2013**, *66*, 2079−2090.
(98) Eslava, S.; Zhang, L.; Esconjauregui, S.; Yang, J.; Vanstreels, K.; Baklanov, M. R.; Saiz, E. Metal-organic framework ZIF-8 films as low-κ dielectrics in microelectronics. *Chem. Mater.* **2013**, *25*, 27−33.
(99) Zhu, M.; Venna, S. R.; Jasinski, J. B.; Carreon, M. A. Room-temperature synthesis of ZIF-8: the coexistence of ZnO nanoneedles. *Chem. Mater.* **2011**, *23*, 3590−3592.
(100) Shekhah, O.; Eddaoudi, M. The liquid phase epitaxy method for the construction of oriented ZIF-8 thin films with controlled growth on functionalized surfaces. *Chem. Commun.* **2013**, *49*, 10079−10081.
(101) Chernikova, V.; Shekhah, O.; Eddaoudi, M. Advanced fabrication method for the preparation of MOF thin films: Liquid-phase epitaxy approach meets spin coating method. *ACS Appl. Mater. Interfaces* **2016**, *8*, 20459−20464.
(102) Mahmoodi, N. M.; Abdi, J. Nanoporous metal-organic framework (MOF-199): Synthesis, characterization and photocatalytic degradation of Basic Blue 41. *Microchem. J.* **2019**, *144*, 436−442.
(103) Sun, B.; Kayal, S.; Chakraborty, A. Study of HKUST (Copper benzene-1, 3, 5-tricarboxylate, Cu-BTC MOF)-1 metal organic frameworks for CH4 adsorption: An experimental Investigation with GCMC (grand canonical Monte-carlo) simulation. *Energy* **2014**, *76*, 419−427.
(104) Li, K.; Fan, Y.; He, Y.; Zeng, L.; Han, X.; Yan, Y. Burkholderia cepacia lipase immobilized on heterofunctional magnetic nanoparticles and its application in biodiesel synthesis. *Scientific reports* **2017**, *7*, 1−17.
(105) Wang, K.; et al. Synthesis and characterization of biodegradable pH-sensitive hydrogel based on poly(ε-caprolactone), methacrylic acid, and Pluronic (L35). *Carbohyd. Polym.* **2010**, *79*, 755−761.
(106) Pu, H. T.; Jiang, F. J.; Yang, Z. L. Preparation and properties of soft magnetic particles based on Fe_3O_4 and hollow polystyrene microsphere composite. *Mater. Chem. Phys.* **2006**, *100*, 10−14.
(107) Wang, P.; Wang, X.; Yu, S.; Zou, Y.; Wang, J.; Chen, Z.; Alharbi, X.; Alsaedi, A.; Hayat, T.; Chen, Y.; Wang, X. Silica coated Fe3O4 magnetic nanospheres for high removal of organic pollutants from wastewater. *Chem. Eng. J.* **2016**, *306*, 280−288.
(108) Chung, T. H.; Pan, H. C.; Lee, W. C. Preparation and application of magnetic poly (styrene-glycidyl methacrylate) micro-spheres. *J. Magn. Magn. Mater.* **2007**, *311*, 36−40.
(109) Shamim, N.; Hong, L.; Hidajat, K.; Uddin, M. S. Thermosensitive-polymer-coated magnetic nanoparticles: adsorption and desorption of bovine serum albumin. *J. Colloid Interface Sci.* **2006**, *304*, 1−8.
(110) Cipolatti, E. P.; Valério, A.; Henriques, R. O.; Moritz, D. E.; Ninow, J. L.; Freire, D. M.; Manoel, D.; Fernandez-Lafuente, R.; de Oliveira, D. Nanomaterials for biocatalyst immobilization−state of the art and future trends. *RSC Adv.* **2016**, *6*, 104675−104692.
(111) Xie, W.; Ma, N. Immobilized lipase on Fe_3O_4 nanoparticles as biocatalyst for biodiesel production. *Energy Fuels* **2009**, *23*, 1347−1353.
(112) Fan, Y.; Wu, G.; Su, F.; Li, K.; Xu, L.; Han, X.; Yan, Y. Lipase oriented-immobilized on dendrimer-coated magnetic multi-walled carbon nanotubes toward catalyzing biodiesel production from waste vegetable oil. *Fuel* **2016**, *178*, 172−178.
(113) Huang, Z.; Xi, L.; Subhani, Q.; Yan, W.; Guo, W.; Zhu, Y. Covalent functionalization of multi-walled carbon nanotubes with quaternary ammonium groups and its application in ion chromatography. *Carbon* **2013**, *62*, 127−134.
(114) Jin, X.; Li, J. F.; Huang, P. Y.; Dong, X. Y.; Guo, L. L.; Yang, L.; Cao, H.; Wei, F.; Zhao, Y.-D.; Chen, H. Immobilized protease on the magnetic nanoparticles used for the hydrolysis of rapeseed meals. *J. Magn. Magn. Mater.* **2010**, *322*, 2031−2037.
(115) Fan, Y.; Su, F.; Li, K.; Ke, C.; Yan, Y. Carbon nanotube filled with magnetic iron oxide and modified with polyamidoamine dendrimers for immobilizing lipase toward application in biodiesel production. *Scientific reports* **2017**, *7*, 1−13.
(116) Yong, Y.; Bai, Y.; Li, Y.; Lin, L.; Cui, Y.; Xia, C. Preparation and application of polymer-grafted magnetic nanoparticles for lipase immobilization. *J. Magn. Magn. Mater.* **2008**, *320*, 2350−2355.
(117) Lei, L.; Liu, X.; Li, Y.; Cui, Y.; Yang, Y.; Qin, G. Study on synthesis of poly (GMA)-grafted Fe3O4/SiOX magnetic nanoparticles using atom transfer radical polymerization and their application for lipase immobilization. *Mater. Chem. Phys.* **2011**, *125*, 866−871.
(118) Shimada, Y.; Watanabe, Y.; Sugihara, A.; Tominaga, Y. Enzymatic alcoholysis for biodiesel fuel production and application of the reaction to oil processing. *J. Mol. Catal. B: Enzym.* **2002**, *17*, 133−142.
(119) Lu, J.; Chen, Y.; Wang, F.; Tan, T. Effect of water on methanolysis of glycerol trioleate catalyzed by immobilized lipase Candida sp. 99−125 in organic solvent system. *J. Mol. Catal. B: Enzym.* **2009**, *56*, 122−125.
(120) You, Q.; Yin, X.; Zhao, Y.; Zhang, Y. Biodiesel production from jatropha oil catalyzed by immobilized Burkholderia cepacia lipase on modified attapulgite. *Bioresour. Technol.* **2013**, *148*, 202−207.
(121) Karimi, M. Immobilization of lipase onto mesoporous magnetic nanoparticles for enzymatic synthesis of biodiesel. *Biocatal. Agric. Biotechnol.* **2016**, *8*, 182−188.
(122) Jegannathan, K. R.; Jun-Yee, L.; Chan, E. S.; Ravindra, P. Production of biodiesel from palm oil using liquid core lipase encapsulated in κ-carrageenan. *Fuel* **2010**, *89*, 2272−2277.
(123) Barbosa, O.; Ortiz, C.; Berenguer-Murcia, Á.; Torres, R.; Rodrigues, R. C.; Fernandez-Lafuente, R. Strategies for the one-step immobilization−purification of enzymes as industrial biocatalysts. *Biotechnol. Adv.* **2015**, *33*, 435−456.
(124) Kumar, D.; Das, T.; Giri, B. S.; Rene, E. R.; Verma, B. Biodiesel production from hybrid non-edible oil using bio-support beads immobilized with lipase from Pseudomonas cepacia. *Fuel* **2019**, *255*, 115801.
(125) Raman, L. A.; Deepanraj, B.; Rajakumar, S.; Sivasubramanian, V. Experimental investigation on performance, combustion and emission analysis of a direct injection diesel engine fuelled with rapeseed oil biodiesel. *Fuel* **2019**, *246*, 69−74.
(126) Sharma, Y. C.; Singh, B. A hybrid feedstock for a very efficient preparation of biodiesel. *Fuel Process. Technol.* **2010**, *91*, 1267−1273.
(127) de Almeida, V. F.; García-Moreno, P. J.; Guadix, A.; Guadix, E. M. Biodiesel production from mixtures of waste fish oil, palm oil and waste frying oil: Optimization of fuel properties. *Fuel Process. Technol.* **2015**, *133*, 152−160.
(128) Chen, Y. H.; Chen, J. H.; Chang, C. Y.; Chang, C. C. Biodiesel production from tung (Vernicia montana) oil and its blending properties in different fatty acid compositions. *Bioresour. Technol.* **2010**, *101*, 9521−9526.
(129) Shah, S.; Gupta, M. N. Lipase catalyzed preparation of biodiesel from Jatropha oil in a solvent free system. *Process Biochem.* **2007**, *42*, 409−414.
(130) Salis, A.; Pinna, M.; Monduzzi, M.; Solinas, V. Comparison among immobilised lipases on macroporous polypropylene toward biodiesel synthesis. *J. Mol. Catal. B: Enzym.* **2008**, *54*, 19−26.
(131) Knothe, G. Dependence of biodiesel fuel properties on the structure of fatty acid alkyl esters. *Fuel Process. Technol.* **2005**, *86*, 1059−1070.
(132) Medina, V. J.; Carrillo, M. G.; Ramirez, O. J. Method to monitor the yield and content of methyl esters in biodiesel using IR vibrational spectroscopy. *University Act* **2011**, *21*, 27−32.

https://doi.org/10.1021/acsomega.2c02873
ACS Omega 2022, 7, 41882−41904

(133) Ortiz Tapia, M. D. C.; García Alamilla, P.; Lagunes Gálvez, L. M.; Arregoitia Quezada, M. I.; García Alamilla, R.; León Chávez, M. A. Obtaining biodiesel from crude palm oil (Elaeis guineensis Jacq.). Application of the ascending route method. *Acta Universitaria Multidisciplinary Scientific Journal* **2016**, *26*, 3−10.
(134) Barabás, I.; Todoruţ, I. A.*Biodiesel quality, standards and properties. Biodiesel-quality, emissions and by-products*: Biodiesel, 2011, pp 3−28.
(135) Sayyed Siraj, R.; Gitte, B. M.; Joshi, S. D.; Dharmadhikari, H. M.Characterization of biodiesel: a review. *Int J Eng Res Technol*, **2013**, *2* DOI: 10.17577/IJERTV2IS100795. ISSN: 2278-0181.
(136) Ong'era, C. M.; Gathitu, BB.; Murunga, SI.; Kuloba, PW.; Gathirwa, J. W.*Caracterización del aceite de colza nanoestructurado como biodíesel de automoción. En Actas de la Conferencia sobre Investigación e Innovación Sostenible*, 2022.(abril de 2022), pp. 33−38. https://sri.jkuat.ac.ke/jkuatsri/index.php/sri/article/view/271/254.
(137) Shumi, L. D.; Waday, YA.; Birru, M. A.*Statistical modeling and optimization of biodiesel production from cherimoya seed oil and characterization*, 2022. https://orcid.org/0000-0002-8830-0176.
(138) Yang, Y.; Wei, Y.; Li, J.; Chen, B.; Ma, W.; Liu, W. Replacing liquid chromatography with custom ion chromatography: an environmentally friendly method to detect furfuryl alcohol and understand its properties. *Chromatography Journal A* **2022**, *1673*, 463090.
(139) Lemke, K.; Lemke, M.; Theil, F. A three-dimensional predictive active site model for lipase from Pseudomonas cepacia. *J. Inorg. Chem.* **1997**, *62*, 6268−6273.
(140) Wu, S.; Wang, W.; Fang, Y.; Kong, X.; Liu, J. Efficient Friedel−Crafts acylation of anisole over silicotungstic acid modified ZIF-8. *Reaction Kinetics, Mechanisms and Catalysis* **2017**, *122*, 357−367.
(141) Jomekian, A.; Bazooyar, B.; Behbahani, R. M. ZIF-8 modified by Pluronic P123 copolymer with enlarged pores and enhanced textural properties for CO_2/CH_4 and CO_2/N_2 separations. *J. Solid State Chem.* **2020**, *289*, 121532.
(142) Chen, M.; Chen, J.; Liu, Y.; Liu, J.; Li, L.; Yang, B.; Ma, L. Enhanced adsorption of thiophene with the GO-modified bimetallic organic framework Ni-MOF-199. *Colloids and Surfaces A: Physicochemical and Engineering Aspects* **2019**, *578*, 123553.
(143) Zhang, H. Y.; Yang, C.; Geng, Q.; Fan, H. L.; Wang, B. J.; Wu, M. M.; Tian, Z. Adsorption of hydrogen sulfide by amine-functionalized metal organic framework (MOF-199): An experimental and simulation study. *Appl. Surf. Sci.* **2019**, *497*, 143815.

https://doi.org/10.1021/acsomega.2c02873
ACS Omega 2022, 7, 41882−41904